

Chapter 12

Numerical Case Studies



12.1 Wave Propagation in a Stepped Bar

12.1.1 Problem Definition

As the first numerical example, wave propagation in an infinite stepped bar of the circular cross-section is considered. It is assumed that only longitudinal elastic waves can propagate within the bar. It is also assumed that the bar is made out of aluminium having the already known material properties: Young's modulus E of 67.5 GPa, Poisson's ratio ν of 0.33 and material density ρ of 2700 kg/m³, also summarised in Table 4.2 in Sect. 4.2. The geometry of the bar under investigation is presented in Fig. 12.1.

A finite section of the bar, having length L_1 of 600 mm, is of particular interest. This section is indicated by points P_1 and P_2 as the points where dynamic responses of the bar are examined. The excitation signal is applied as a longitudinally acting force at point P_1 , having the amplitude of 1 N and the form of 5 sine pulses at the carrier frequency f_c of 166.7 kHz, modulated by the Hann window, i.e. the frequency of modulation $f_m = f_c/m$ being equal to 33.3 kHz, where $m = 5$. The total calculation time T covers 300 μ s and is divided into 6,000 equal time steps. The excitation signal is presented in Fig. 12.2 in the time and frequency domains, for the initial 100 μ s of its duration in the time domain and the frequency range up to 500 kHz in the frequency domain.

As clearly seen from Fig. 12.2b the excitation signal is broad in the frequency domain covering frequencies from the range starting at $f_1 = 100.0$ kHz up to $f_2 = 233.3$ kHz, where $f_{1,2} = f_c \mp 2f_m$. It should be recalled that within this frequency range 97% of the signal energy is stored, as discussed earlier in Sect. 2.5.

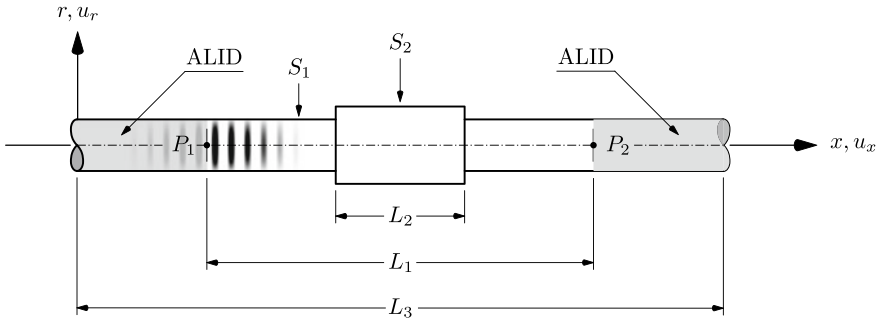


Fig. 12.1 Geometry of an infinite stepped aluminium bar with NRCBs at infinity modelled by ALID

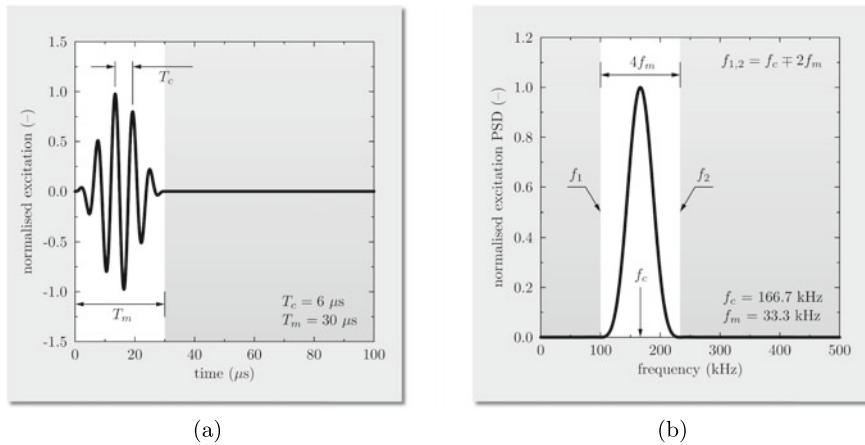


Fig. 12.2 Normalised excitation signal in: **a** the time domain, **b** in the frequency domain

The stepped bar under consideration can be characterised by two different cross-sectional areas, as clearly seen in Fig. 12.1. The cross-sectional area of the bar is $S_1 = \pi R_1^2$ over its entire length except a short section having length L_3 of 200 mm, where the cross-sectional area is increased to $S_2 = \pi R_2^2$. The assumed values of the radii R_1 and R_2 are 5 and 7 mm, respectively.

12.1.2 Dispersion Curves and Theory Selection

For modes of longitudinal waves propagating within the bar, the wide range of excited frequencies must be compared with the analytical dispersion curves already known from Sect. 6.1, in order to select the most appropriate theory of longitudinal behaviour of rods, which next can be employed for numerical computations.

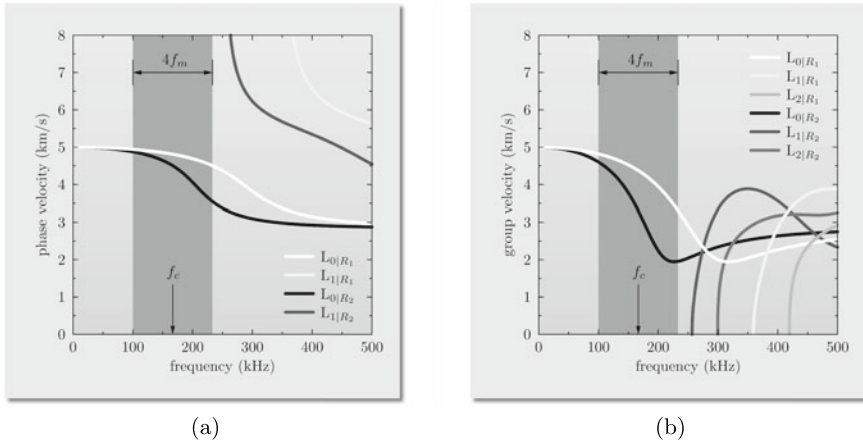


Fig. 12.3 Dispersion curves for: **a** the phase velocity, **b** the group velocity, for modes of longitudinal waves L_n ($n = 0, 1, 2$) corresponding to both cross-sectional areas of an infinite stepped aluminium bar, according to the analytical solution

It is clear from Figs. 12.1 and 12.2 that excited elastic longitudinal waves cover different ranges of wave velocities for each cross-sectional area of the bar. According to the analytical solutions presented in Sect. 6.1, in the case of the cross-sectional area S_1 this range covers phase velocities from 4.94 km/s at $f_1 = 100.0$ kHz down to 4.51 km/s at $f_2 = 233.3$ kHz, while in the case of the cross-sectional area S_2 , phase velocities from 4.88 km/s at $f_1 = 100.0$ kHz down to 3.55 km/s at $f_2 = 233.3$ kHz, respectively.

In a similar manner to the case of the cross-sectional area S_1 the same range of frequencies covers group velocities from 4.82 km/s at $f_1 = 100.0$ kHz up to 3.31 km/s at $f_2 = 233.3$ kHz, while in the case of the cross-sectional area S_2 , group velocities from 4.01 km/s at $f_1 = 100.0$ kHz up to 1.96 km/s at $f_2 = 233.3$ kHz, respectively. This is clearly illustrated in Fig. 12.3.

As clearly seen from Fig. 12.3 the longitudinal waves propagating in 1-D elastic space, which is the infinite stepped aluminium bar under consideration, are characterised by *very strong dispersion*,¹ i.e. -8.7% of the relative change in the phase velocity and -31% in the group velocity in the case of the cross-sectional area S_1 , as well as -27% of the relative change in the phase velocity and -51% in the group velocity in the case of the cross-sectional area S_2 . This dispersion directly results from the Pochhammer characteristic equation and the broad range of excited frequencies. Moreover, it practically concerns the fundamental longitudinal mode L_0 ,

¹ It is convenient to assume wave signals as characterised by dispersion of various strengths: very small, small, moderate, strong and very strong. These strengths correspond to absolute levels of the relative change in their phase or group velocities over a given frequency range, i.e. less than 1% for very small, up to 5% for small, up to 10% for moderate, up to 20% for strong and above 30% for very strong dispersion.

which is denoted as $L_{0|R_1}$ in the case of the cross-sectional area S_1 and as $L_{0|R_2}$ in the case of the cross-sectional area S_2 . A similar notation is used for higher longitudinal modes L_1 and L_2 .

Moreover, it was clearly indicated in Fig. 9.10 from Sect. 9.1 that in the case of very strong dispersion, multi-mode or higher-order multi-mode theories of the longitudinal behaviour of rods prove to be more useful due to small relative modelling errors, as also summarised in Table 9.1. It is seen that in the current case the upper frequency limit of the excitation signal never exceeds the frequency corresponding to the first cut-off frequency $f_{L_1|R_1}$ of 359.4 kHz in the case of the cross-sectional area S_1 and $f_{L_1|R_2}$ of 256.7 kHz in the case of the cross-sectional area S_2 . For this reason it is decided to employ *the higher-order 2-mode 2-D theory of rod behaviour* for the purpose of numerical modelling. This theory can be characterised by relatively simple definition of its displacement field and a great accuracy in the frequency range of interest. It should be emphasised here that the values of the cut-off frequencies based on analytical dispersion curves are always lower than the corresponding values obtained as based on simplified theories, providing a kind of safe margin in modelling.

The phase velocity dispersion curves obtained for the selected theory, for modes of longitudinal waves $L_{0|R_1}$ and $L_{1|R_1}$ as well as $L_{0|R_2}$ and $L_{1|R_2}$, corresponding to both cross-sectional areas S_1 and S_2 of the bar under consideration, are presented in Fig. 12.4.

Indeed, it can be checked that within the range of excited frequencies the dispersion curves for the fundamental mode of longitudinal waves L_0 , corresponding to both cross-sectional areas of the bar, obtained for the selected higher-order 2-mode 2-D theory of the longitudinal behaviour of rods, agree very well with the analytical solutions obtained based on the Pochhammer characteristic equation. In the case of

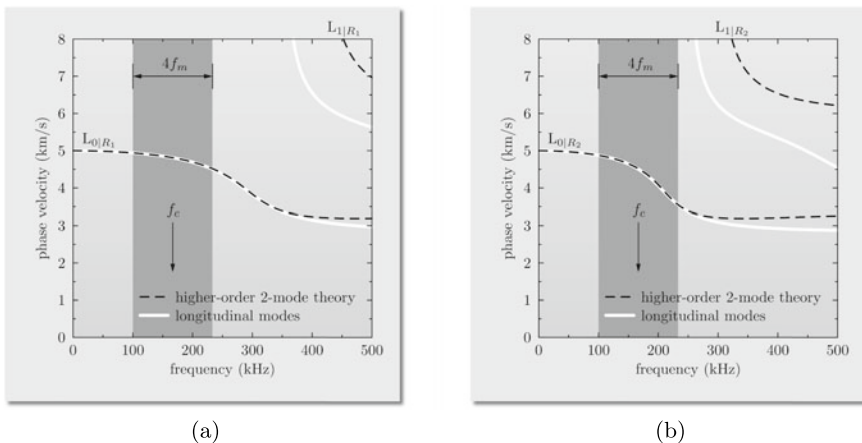


Fig. 12.4 Dispersion curves for the phase velocity for modes of longitudinal waves L_0 and L_1 , corresponding to: **a** the cross-sectional area S_1 , **b** the cross-sectional area S_2 , of an infinite stepped aluminum bar, according to the higher-order 2-mode 2-D theory of the longitudinal behaviour of rods

the cross-sectional area S_1 the extreme value of the relative modelling error associated with the phase velocity is negligible, since its value is equal to 0.26%, while its average value to 0.06%. In the case of the cross-sectional area S_2 the extreme value of the relative modelling error is higher, but still very small, and is equal to 0.60%, while its average value to 0.22%.

In order to mimic the infinite length of the bar the technique of ALID is used, discussed in detail in Sect. 11.3. As a consequence of this the numerical model must be extended² accordingly in order to incorporate the presence of two damping layers, one at each end of the bar, as presented in Fig. 12.1. The depths of the layers must be defined as resulting not only from the frequency content of the excitation signal, but also as depending on the applied theory.

12.1.3 ALID Parameters and Numerical Discretisation

It is noteworthy that the knowledge of the range of excited frequencies can be used not only in order to select the most appropriate theory of the longitudinal behaviour of rods, or to establish the depth of ALID, but also to establish the requirements for the bar discretisation conforming with the minimal number of nodal distances per wavelength. The dispersion curves for the wavelength for modes of longitudinal waves corresponding to both cross-sectional areas of the bar, according to the higher-order 2-mode theory of the longitudinal behaviour of rods, are presented in Fig. 12.5.

It can be clearly seen from Fig. 12.5 that in the case of the cross-sectional area S_1 the extreme wavelengths for the selected excitation signal and its frequency content are $\lambda_{1|R_1} = 49.4$ mm at the frequency $f_1 = 100.0$ kHz and $\lambda_{2|R_1} = 19.4$ m at the frequency $f_2 = 233.3$ kHz. In a similar manner in the case of the cross-sectional area S_2 the corresponding wavelengths are $\lambda_{1|R_2} = 48.8$ mm at the frequency $f_1 = 100.0$ kHz and $\lambda_{1|R_2} = 15.2$ m at the frequency of $f_2 = 233.3$ kHz. Since the presence of ALID solely concerns the cross-sectional area S_1 the depth of each damping layer should be selected as a multiple of $\lambda_{1|R_1} = 49.4$ mm, so the assumed depth of ALID is $L = 4\lambda_{1|R_1} \approx 200$ mm, with $p = 3$. For this reason the total length of the bar under consideration is increased by $2L$ from $L_2 = 600$ mm to $L_3 = 1000$ mm.

It also is evident from Fig. 12.5 that the cut-off frequencies $f_{L_1|R_1}$ and $f_{L_1|R_2}$ corresponding to the current higher-order 2-D theory of the longitudinal behaviour of rods are greater than those corresponding to the analytical solution based on the Pochhammer characteristic equation. In the case of the cross-sectional area S_1 this value is equal to 419.3 kHz, while in the case of the cross-sectional area S_2 it is equal to 299.5 kHz.

At this point it should be strongly emphasised that any changes in the excitation frequency f_c or the modulation frequency f_m must involve corresponding modifi-

² In order to mimic the behaviour of an infinite bar by the direct approach the enlarged FE model should be approximately 3 times greater to guarantee no reflections from the external boundaries within the assumed time window.

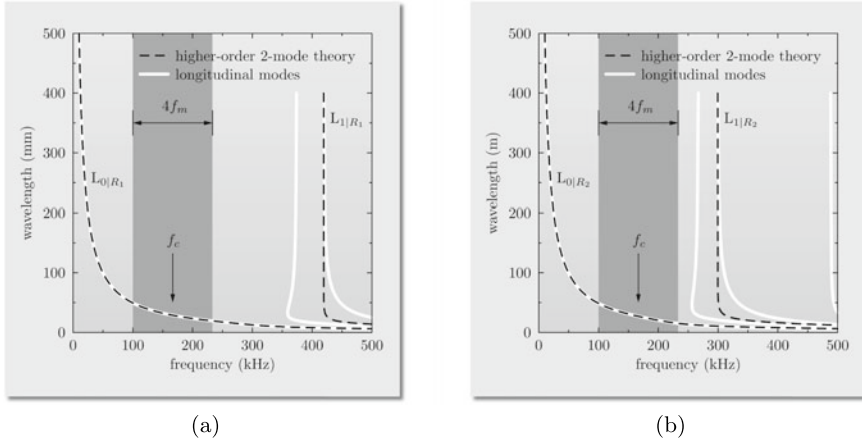


Fig. 12.5 Dispersion curves for the wavelength for modes of longitudinal waves L_0 and L_1 , corresponding to: **a** the cross-sectional area S_1 , **b** the cross-sectional area S_2 , of an infinite stepped aluminium bar, according to the higher-order 2-mode 2-D theory of the longitudinal behaviour of rods

cations to the depth of ALID in order to guarantee its optimal damping properties. Based on the established parameters of ALID and the requirements for rod discretisation a numerical model of the stepped bar under investigation can be finally built. For the purpose of the current analysis it is decided to use TD-SFEM and 6-node rod SFEs based on Chebyshev nodes [1], as discussed in Sect. 10.4.

The knowledge of the corresponding shortest wavelengths obtained from Fig. 12.5 allows one to state that in the case of the cross-sectional area S_1 the requirement of 5 nodal distances per wavelength is satisfied only for the lengths of SFEs equal³ to or shorter than the wavelength $\lambda_{2|R_1} = 19.4$ mm, while in the case of the cross-sectional area S_2 for the lengths of SFEs equal to or shorter than the wavelength $\lambda_{2|R_2} = 15.2$ mm. Since it is decided to divide the bar into 500 rod SFEs of equal lengths, with the resulting length l of a single rod SFE equal to 2 mm, the number of nodal distances per wavelength secured by such a discretisation level can be estimated as approximately equal to 48 nodal distances in the case of the cross-sectional area S_1 and 38 nodal distances in the case of the cross-sectional area S_2 , respectively. The resulting number of the discrete numerical model DOFs is 5,002.

12.1.4 Numerical Computations and Result Discussion

For numerical computations carried out the implicit β -Newmark method is used, as discussed in Sect. 10.7, for the recommended values of the parameters α and β

³ It is because for 6-node SFEs there are always 4 nodal distances between their first and last nodes.

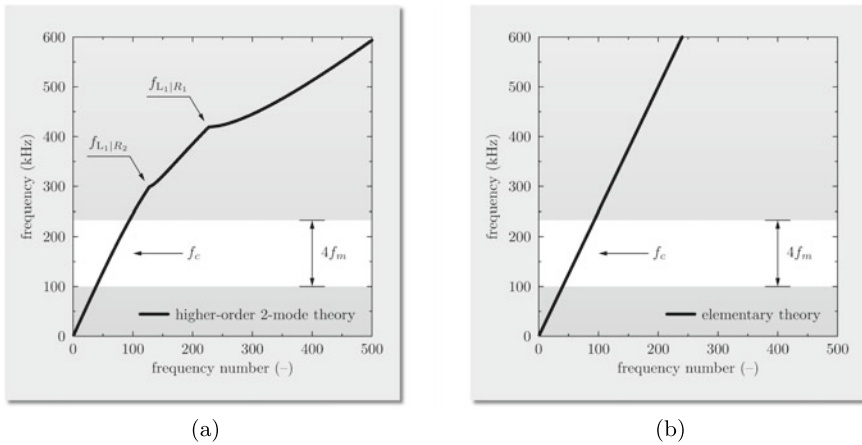


Fig. 12.6 Spectra of frequencies of free vibrations for modes of longitudinal waves, corresponding to: **a** the higher-order 2-mode 2-D theory, **b** the 1-mode 1-D (elementary) theory, of the longitudinal behaviour of rods, obtained for an infinite stepped aluminium bar. Results of numerical computations by TD-SFEM with NRBCs at infinity modelled by ALID

equal to $1/2$ and $1/4$, respectively. However, prior to the solution of the equations of motion the spectrum of frequencies of free vibrations of the bar under investigation is examined to confirm the correctness of the assumed parameters of the discrete numerical model of the bar, as presented in Fig. 12.6.

It should be noted that in this step the discrete numerical model of the bar must take into account the contributions to the characteristic global inertia matrix \mathbf{M} and the global stiffness matrix \mathbf{K} resulting from the presence of both damping layers. For the sake of comparison this spectrum is accompanied by the spectrum of frequencies of free vibrations of the same bar, however, obtained in the case of the 1-mode 1-D theory (elementary) of rods. The remaining features and parameters of the discrete numerical model of the bar remain the same.

It can be seen from Fig. 12.6 that the obtained spectrum of frequencies of free vibrations correlates very well with the dispersion curves for the phase velocity, previously presented in Fig. 12.4. At the same time the computational effort related to finding the frequencies of free vibrations, preferably a finite number of them, is much smaller than that corresponding to the process of establishing all dispersion curves from the Pochhammer characteristic equation.

As a final element of the examination of the discrete numerical model the analysis of the performance of ALID is examined, since the use of ALID is directly responsible for the correctness and accuracy of calculated dynamic responses and generally for appropriate mimicking of the infinite dimensions of the bar [2]. The damping properties of ALID are tested in the case of a simplified geometry of the bar under the assumption of the constant cross-sectional area of the bar of S_1 along its entire length. In such a manner the only reflections, which potentially can be present in the

Table 12.1 Statistical data on the relative amplitude damping associated with the ALID performance for the 1-mode 1-D (elementary) and the higher-order 2-mode 2-D theory of longitudinal behaviour of rods

Theory	Component	Disp. (dB)	Vel. (dB)	Acc. (dB)
Elementary 1-D	Longitudinal	42.69	60.32	83.25
Higher-order 2-mode 2-D	Longitudinal	38.52	70.15	82.56
	Radial	74.11	105.9	118.5

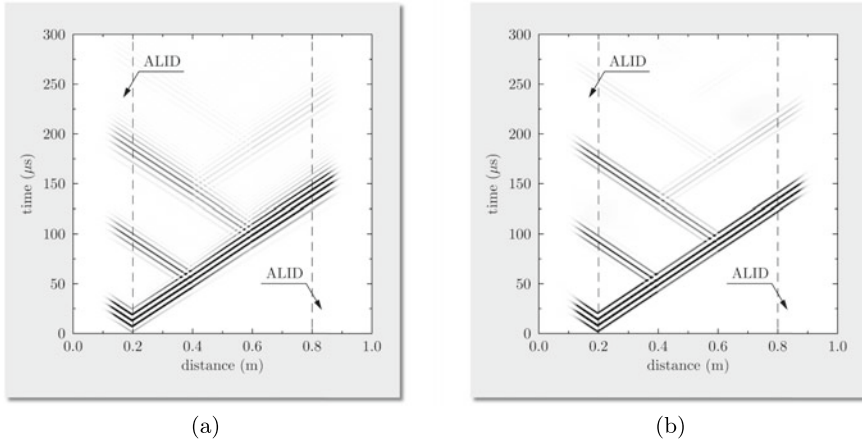


Fig. 12.7 Wave propagation patterns for the longitudinal acceleration component \ddot{u}_x for: **a** the higher-order 2-mode 2-D theory, **b** the 1-mode 1-D (elementary) theory, of the longitudinal behaviour of rods, obtained for an infinite stepped aluminium bar. Results of numerical computations by TD-SFEM with NRBCs at infinity modelled by ALID

calculated dynamic responses are those related to the improper performance of ALID. The obtained results for the assumed form of the excitation signal are summarised in Table 12.1.

Knowledge of the established parameters of the discrete numerical model of the bar under consideration allows one to compute its dynamic responses. They are presented as wave propagation patterns for the longitudinal acceleration component \ddot{u}_x in Fig. 12.7 and compared with similar results obtained in the case of the 1-mode 1-D theory (elementary) of the longitudinal behaviour of rods.⁴ It is also evident from Fig. 12.7 that the wave propagation patterns exhibit regions, when propagating elastic waves interact with the structural discontinuity present, very clearly revealing the part of the bar of the increased cross-sectional area. This concerns both discrete

⁴ In the case of the higher-order 2-mode 2-D theory of the longitudinal behaviour of rods the longitudinal displacement component u_x , or its time derivatives, can be compared with that of the 1-mode 1-D (elementary) theory only on the upper surface of the bar, i.e. for $\zeta = 1$. Note that no such relationship exists for the radial displacement component u_r .

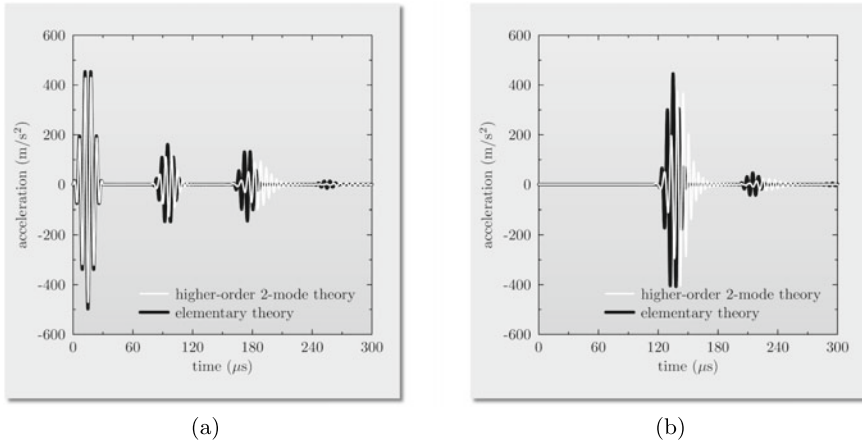


Fig. 12.8 Dynamic responses for the longitudinal acceleration component \ddot{u}_x taken at: **a** point P_1 , **b** point P_2 , of an infinite stepped aluminium bar modelled according to the 1-mode 1-D (elementary) and the higher-order 2-mode 2-D theory of the longitudinal behaviour of rods. Results of numerical computations by TD-SFEM with NRBCs at infinity modelled by ALID

numerical models of the bar. Despite the fact that qualitatively the obtained results are similar, certain obvious differences can be indicated.

It can be stated that the observed differences result from the dispersive nature of the longitudinal waves, which is the direct consequence of the analytical solutions arising from the Pochhammer characteristic equation as well as the frequency content of the excitation signal. Obviously, this feature cannot be mimicked by the 1-mode 1-D (elementary) theory of the longitudinal behaviour of rods, since in the case of this theory the phase and the group velocities remain independent of the frequency as well as the cross-sectional area of the bar. In other words the 1-mode 1-D (elementary) theory is non-dispersive.

The difference between the results obtained based on both discrete numerical models of the bar becomes more apparent and even more strongly emphasised when the dynamic responses obtained are compared at points P_1 and P_2 , as presented in Fig. 12.8, for the longitudinal acceleration component \ddot{u}_x .

Now, it is evident from Figs. 12.7 and 12.8 that this difference builds up in time and distance, which for elongated structural elements may lead to significant discrepancies. Such behaviour may be important for problems related to detection of any structural discontinuities, such as the stepped change in the bar cross-sectional area. For this reason the use of the 1-mode 1-D (elementary) theory for problems involving propagation of elastic waves should practically be limited only to quantitative numerical tests before more appropriate multi-mode or higher-order multi-mode theories are applied.

12.2 Wave Propagation in a Strip with a Side Cut-Out

12.2.1 Problem Definition

In the second numerical example a similar configuration to the previously analysed infinite stepped aluminium bar with NRBC is considered. This time, however, the object of the analysis is an infinite strip with a side cut-out. The geometry of the strip is presented in Fig. 12.9.

It is assumed that as well as flexural waves, also shear horizontal waves can propagate within the strip. It is assumed that the strip is made out of the same material as previously, which is aluminium of the already known material properties: Young's modulus E of 67.5 GPa, Poisson's ratio ν of 0.33 and material density of 2700 kg/m^3 , as summarised in Table 4.2 in Sect. 4.2.

As before a finite section of the strip, having length L_1 of 900 mm, width B_1 of 300 mm and thickness h of 10 mm, is of particular interest. This section is indicated by points P_1 and P_2 as the points where dynamic responses of the strip are examined. The excitation signal is applied at point P_1 as a transversely acting bending force leading to the generation of antisymmetric SH-waves and antisymmetric Lamb waves. The excitation signal is assumed to have the amplitude of 1 N and the form of 12 sine pulses at the carrier frequency f_c of 60 kHz, modulated by the Hann window, i.e. the frequency of modulation $f_m = f_c/m$ being equal to 5 kHz, where $m = 12$. The total calculation time T covers $800 \mu\text{s}$ and is divided into 6400 equal time steps. The

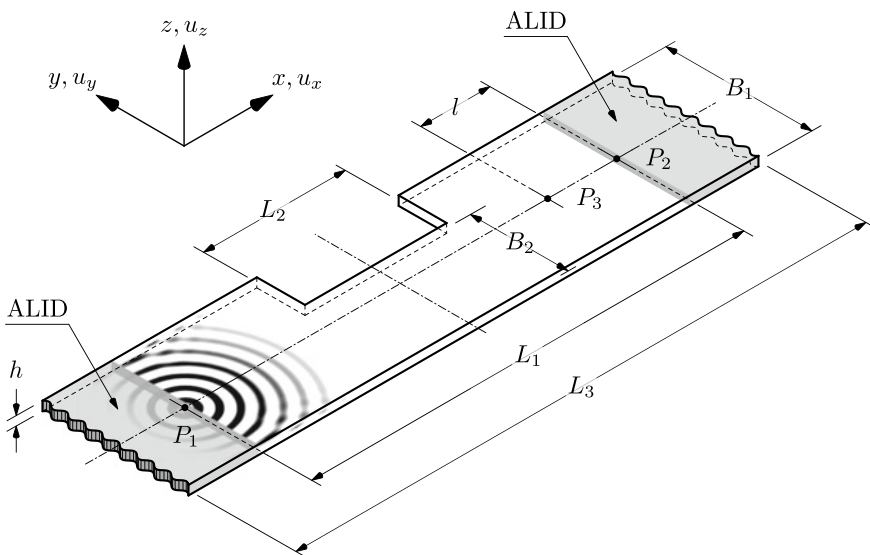


Fig. 12.9 Geometry of an infinite aluminium strip with a side cut-out, with NRCBs at infinity modelled by ALID

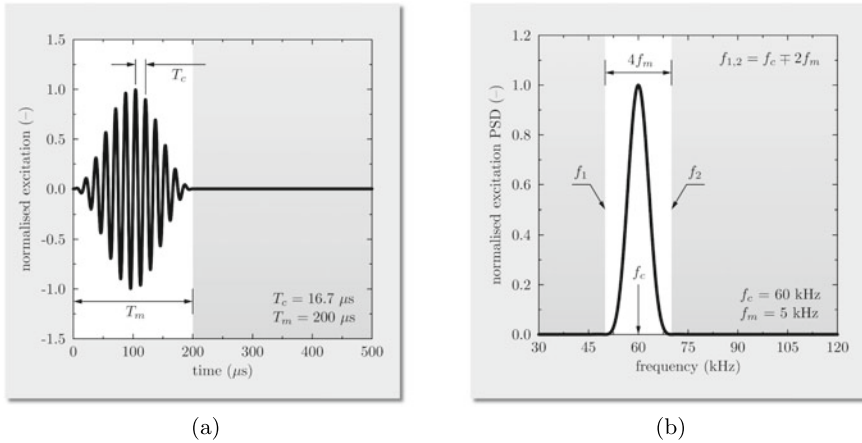


Fig. 12.10 Normalised excitation signal in: **a** the time domain, **b** in the frequency domain

excitation signal is presented in Fig. 12.10 in the time and frequency domains, for the initial 500 μs of its duration in the time domain and the frequency range from 30 kHz up to 120 kHz in the frequency domain.

It is evident from Fig. 12.10b that this time the excitation signal is narrow in the frequency domain covering frequencies from within the range from $f_1 = 50 \text{ kHz}$ up to $f_2 = 70 \text{ kHz}$, where as before $f_{1,2} = f_c \mp 2f_m$. It should be recalled that within this frequency range 97% of the signal energy is stored, as discussed earlier in Sect. 2.5.

From Fig. 12.9 it can be seen that the strip under consideration can be characterised by a stepped change in its width, which is reduced from one side from the initial width B_1 of 300 mm to B_2 of 200 mm, i.e. by the cut-out of depth equal to 100 mm extending over the distance L_2 of 300 mm. Additionally, point P_3 , located at the distance l of 150 mm from point P_2 indicates the position of an additional mass of 5 g. It is noteworthy that the additional mass of 5 g is equivalent to less than 0.1% of the total mass of the strip. The additional mass is assumed to be placed on the upper surface of the strip.

12.2.2 Dispersion Curves and Theory Selection

In a similar manner to before the range of excited frequencies must be compared with the analytical dispersion curves already known from Sects. 5.1 and 5.2, for the antisymmetric modes of SH-waves and the Lamb waves propagating within the strip, in order to select the most appropriate theory of antisymmetric behaviour of plates, which next can be employed for numerical computations.

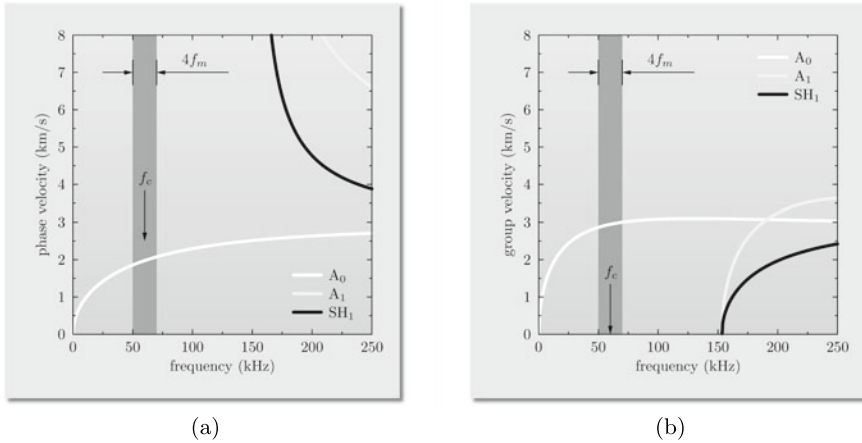


Fig. 12.11 Dispersion curves for: **a** the phase velocity, **b** the group velocity, for antisymmetric modes of Lamb waves and SH-waves: A_0 , A_1 and SH_1 propagating in a 10 mm thick aluminium strip with a side cut-out, according to the analytical solutions

From Figs. 12.9 and 12.10 it is clear that due to the assumed form of the excitation signal the excited waves within the strip practically concern the fundamental antisymmetric mode of Lamb waves A_0 , while the other antisymmetric modes of SH-waves and Lamb waves are absent. According to the analytical solutions presented in Sect. 5.2 the excited phase velocities for the fundamental antisymmetric mode of Lamb waves A_0 cover the range from 1.86 km/s at $f_1 = 50$ kHz up to 2.08 km/s at $f_2 = 70$ kHz, while in the case of the group velocities from 2.87 km/s at $f_1 = 50$ kHz up to 3.01 km/s at $f_2 = 70$ kHz.

Based on Fig. 12.11 it can be concluded that the waves propagating as the fundamental antisymmetric mode of Lamb waves A_0 in 2-D elastic space, which is the infinite aluminium strip under investigation with a side cut-out, are characterised by a moderate dispersion, i.e. 12% of the relative change in the phase velocity and 5% in the group velocity. This is a direct consequence of the characteristic equation for antisymmetric modes of Lamb waves. This, together with the considerations from Sect. 8.2 and the results presented in Fig. 8.20 allow one to state that simple multi-mode theories of the antisymmetric behaviour of plates appears sufficient for modelling purposes, as summarised in Table 8.2.

It is seen that in the current case the upper frequency limit of the excitation signal is placed well below the frequency corresponding to the first cut-off frequency for the first antisymmetric mode of SH-waves and Lamb waves A_1 and SH_1 , $f_{A_1|SH_1}$ of 153.4 kHz. For this reason it is decided to employ the modified 3-mode 2-D theory of antisymmetric behaviour of plates. This theory is characterised by a simple definition of its displacement field combined with the greatest accuracy in the frequency range of interest out of the theories discussed in Sect. 8.2. As before it should be emphasised that the values of the cut-off frequencies provided by analytical dispersion curves

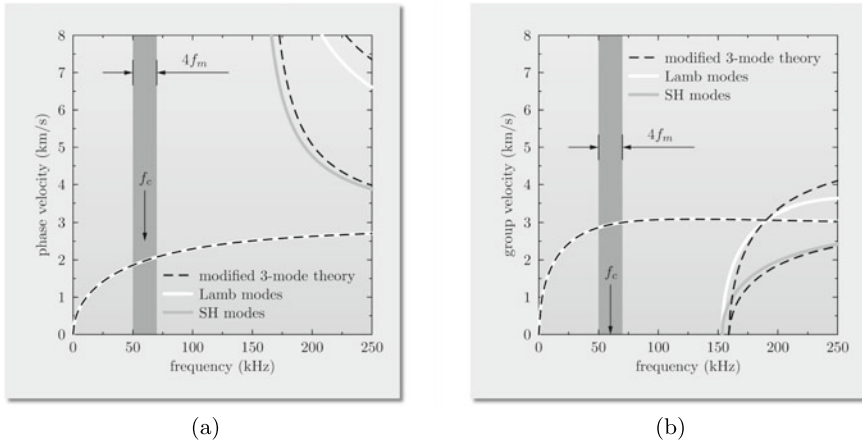


Fig. 12.12 Dispersion curves for: **a** the phase velocity, **b** the group velocity, for antisymmetric modes of Lamb waves and SH-waves propagating in a 10 mm thick infinite aluminium strip with a side cut-out, according to the modified 3-mode 2-D theory of the antisymmetric behaviour of plates

are always lower than the values obtained from simplified theories, thus providing a kind of safe margin in modelling.

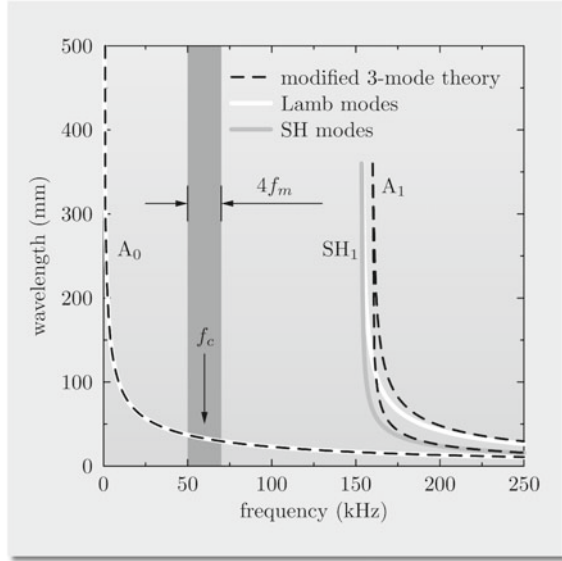
The phase and group velocity dispersion curves obtained for this theory, for antisymmetric modes of Lamb waves and SH-waves, are presented in Fig. 12.12. It can be clearly seen Fig. 12.12 that within the range of excited frequencies the dispersion curve for the fundamental antisymmetric mode of Lamb waves A_0 , obtained for the selected modified 3-mode 2-D theory of the antisymmetric behaviour of plates, agrees very well with the analytical solution obtained based on the characteristic equation.

The results presented in Fig. 12.12 allow one to easily assess the values of the modelling error. In the case of the fundamental antisymmetric mode of Lamb waves A_0 it can be checked that the extreme value of the modelling error associated with the phase velocity is negligible with its value equal to 0.03% and its average value to 0.02%. In a similar manner the extreme value of the modelling error associated with the group velocity is equal to -0.10% and its average value to -0.06% .

12.2.3 ALID Parameters and Numerical Discretisation

In order to model the infinite length of the strip the same method is employed in the current case as in the case of the infinite stepped aluminium bar, which is the technique of ALID, discussed in detail in Sect. 11.3. As before a consequence of the use of ALID is that the numerical model of the strip must be extended accordingly to incorporate the presence of two damping layers, one at each end of the strip, as

Fig. 12.13 Dispersion curves for the wavelength for modes of Lamb waves and SH-waves of a 10 mm thick infinite aluminium strip with a side cut-out, according to the modified 3-mode 2-D theory of the antisymmetric behaviour of plates



presented in Fig. 12.9. The depths of the layers must be defined as resulting not only from the frequency content of the excitation signal, but also as depending on the applied theory.

Again, it can be stated that the knowledge of the range of the excited frequencies can be used not only to select the most appropriate theory of the antisymmetric behaviour of plates or to establish the depth of ALID, but also to establish the requirements for the strip discretisation conforming with the minimal number of nodal distances per wavelength. The dispersion curves for the wavelength for modes of Lamb waves and SH-waves, according to the modified 3-mode 2-D theory of the antisymmetric behaviour of plates, are presented in Fig. 12.13.

It can be clearly seen from Fig. 12.13 that the extreme wavelengths for the selected excitation signal and its frequency content are $\lambda_1 = 37.1$ mm at the frequency $f_1 = 50$ kHz and $\lambda_2 = 29.7$ mm at the frequency $f_2 = 70$ kHz. Since the presence of ALID solely concerns the fundamental antisymmetric mode of Lamb waves A_0 the depth of each damping layer should be selected as a multiple of $\lambda_1 = 37.1$ mm, so the assumed depth of ALID is $L = 4\lambda_1 \approx 150$ mm, with $p = 3$. For this reason the total length of the strip under consideration is increased by $2L$ from $L_2 = 900$ mm to $L_3 = 1200$ mm.

Yet again it should be strongly emphasised that any changes in the excitation frequency f_c or the modulation frequency f_m must involve corresponding modifications to the depth of ALID in order to guarantee its optimal damping properties. Based on the established parameters of ALID and the requirements for plate discretisation a numerical model of the strip under investigation with a side cut-out can be finally

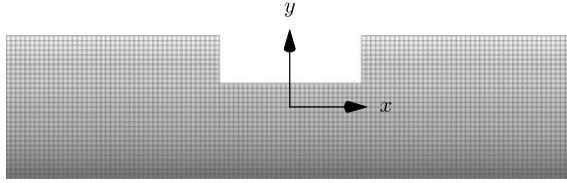


Fig. 12.14 The mesh of plate SFEs, according to the modified 3-mode 2-D theory of the antisymmetric behaviour of plates, used for numerical computations, consisting of 3,300 SFEs and 249,903 DOFs

built. For the purpose of the current analysis it is decided to use TD-SFEM and 36-node plate SFEs based on Lobatto nodes [1], as discussed in Sect. 10.4.

The knowledge of the corresponding shortest wavelengths obtained from Fig. 12.13 allows one to state, in a similar manner as in the case of the stepped aluminium bar, that the requirement of 5 nodal distances per wavelength is satisfied only for the characteristic dimensions of FEs equal to or shorter than the wavelength $\lambda_2 = 29.7$ mm. Thus, it is decided to divide the strip into 3,300 plate SFEs, i.e. 120 SFEs along its length axis and 30 SFEs along its width, excluding 300 SFEs resulting from the presence of the cut-out. The mesh of SFEs resulting from the discretisation process is presented in Fig. 12.14. All SFEs represent squares of equal dimensions of 10 by 10 mm. Since the characteristic dimension of a single plate SFE is 10 mm, the number of nodal distances per wavelength secured by such a discretisation level can be estimated as approximately equal to 15 nodal distances per shortest wavelength. The resulting number of DOFs of the discrete numerical model is 249,903.

12.2.4 Numerical Computations and Result Discussion

For numerical computations carried out the explicit method of central differences is used, as discussed in Sect. 10.7. The use of the explicit method of central differences enables one to take full advantage of the diagonal form of the resulting global inertia matrix \mathbf{M} . It is noteworthy that in the current case however, the spectrum of frequencies of free vibrations of the strip is not examined due to the 2-D nature of the strip and, resulting from this, couplings of normal modes, which significantly complicate such an analysis in comparison with a 1-D case. For the very same reason also the performance of ALID is not tested. This performance can only be estimated based on the methodology presented before and concerning the results obtained in the case of the 1-D infinite stepped aluminium bar.

The knowledge of the established parameters of the discrete numerical model of the strip under consideration allows one to compute its dynamic responses. They are presented in Fig. 12.15 as wave propagation patterns at selected moments in time for the transverse acceleration component \ddot{u}_z . It can be expected that the interaction of propagating waves with a structural discontinuity in the form of the additional

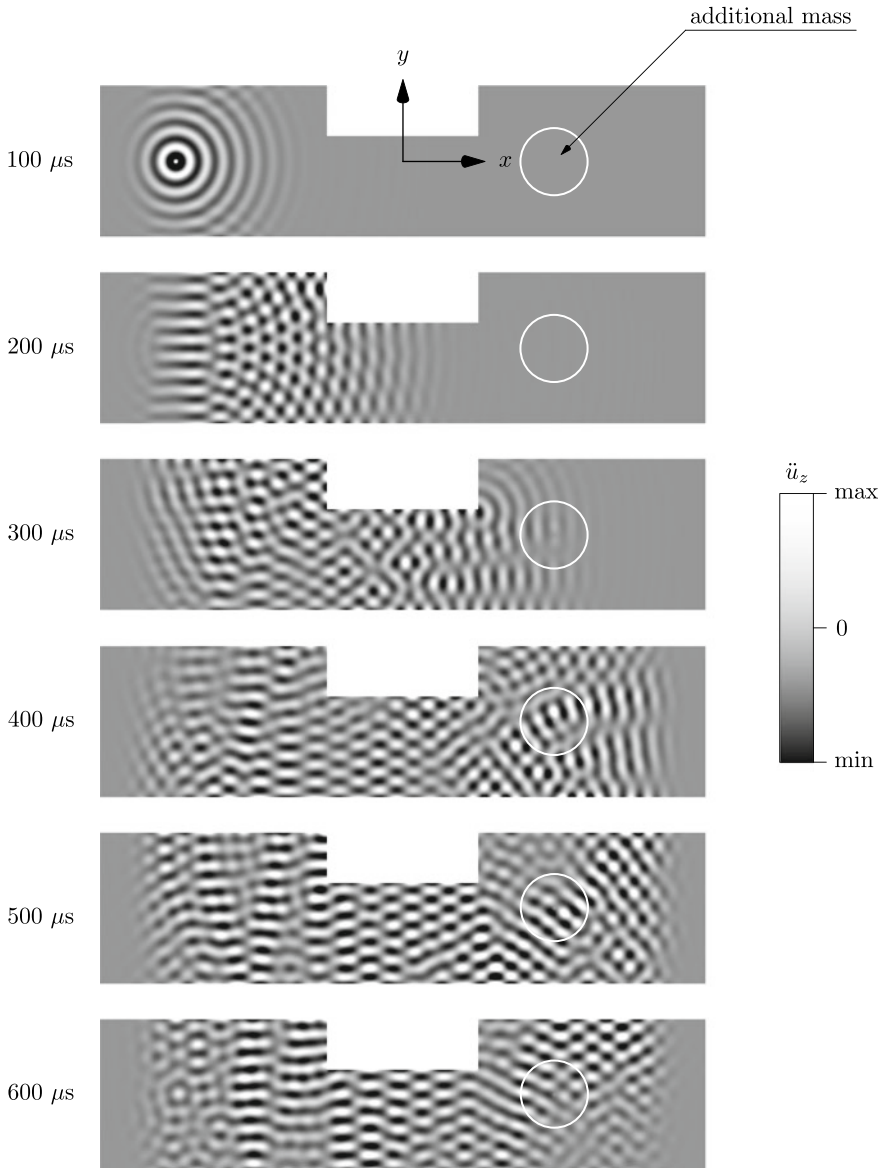


Fig. 12.15 Wave propagation patterns for the transverse acceleration component \ddot{u}_z according to the modified 3-mode 2-D theory of the antisymmetric behaviour of plates, obtained for a 10 mm thick infinite aluminium strip with a side cut-out. Results of numerical computations by TD-SFEM with NRBCs at infinity modelled by ALID

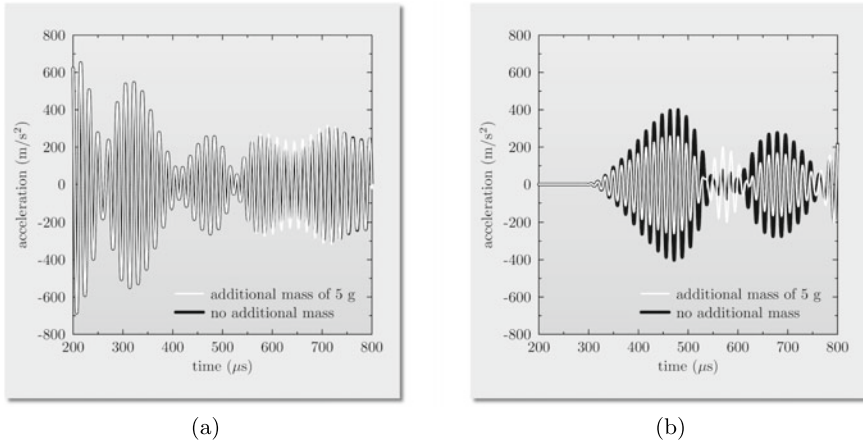


Fig. 12.16 Dynamic responses for the transverse acceleration component \ddot{u}_x taken at: **a** point P_1 , **b** point P_2 , of an infinite aluminium strip with a side cut-out modelled according to the modified 3-mode 2-D theory of the antisymmetric behaviour of plates. Results of numerical computations by TD-SFEM with NRBCs at infinity modelled by ALID

mass should influence the observed patterns in such a way that the location of the additional mass is clearly revealed. However, from the results presented in Fig. 12.15 this is not evident.

The reason for such behaviour may seem to lay in too small sensitivity of the propagating waves to structural damage/discontinuity. This sensitivity may be estimated as proportional to the shortest wavelength out of all wavelengths constituent in the propagating waves and resulting from the assumed form of the excitation signal, which in the current case is $\lambda_2 = 29.7$ mm. However, this is not applicable to damage/discontinuity represented by a point mass. Alternatively, the problem may also be related to too complicated wave propagation patterns, which are very difficult to interpret due to multiple reflections and/or possible mode conversion. This problem is very well illustrated by Fig. 12.16 where the obtained dynamic responses are compared at points P_1 and P_2 . It should be stressed that since the dynamic responses obtained at point P_1 are initially dominated by the excitation, it is decided to exclude the time window corresponding to the duration of excitation, which is equal to the modulation time T_m of 200 μs.

It can be seen from Fig. 12.16 that within the time signals corresponding to points P_1 and P_2 there is no clear evidence of any reflections resulting from the presence of the additional mass, which on the other hand is the effect of signal reflections from lateral structural boundaries. Despite the fact that the signals obtained for the case when the additional mass is present or not must be different, it is impossible to extract directly from them any useful information about the location of the additional mass.

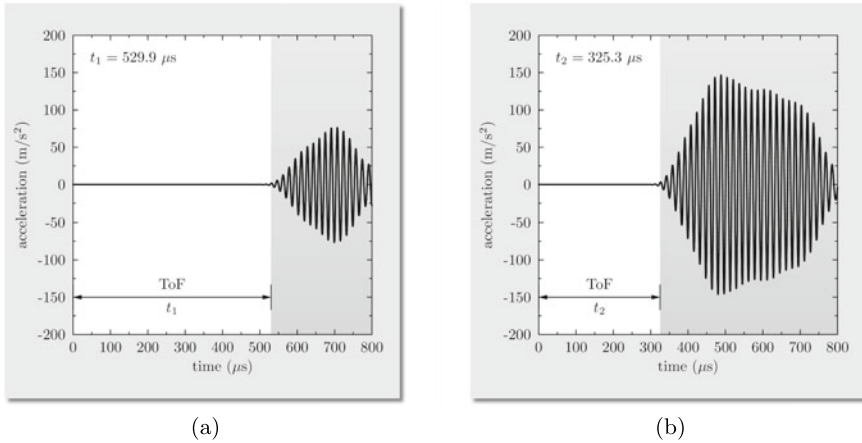


Fig. 12.17 Differential signals for the transverse acceleration component \ddot{u}_x taken at: **a** point P_1 , **b** point P_2 , of an infinite aluminium strip with a side cut-out modelled according to the modified 3-mode 2-D theory of the antisymmetric behaviour of plates. Results of numerical computations by TD-SFEM with NRBCs at infinity modelled by ALID

This adverse situation is not significantly improved when differential signals⁵ are examined, as shown in Fig. 12.17. It is clear that the amplitudes of the differential signals corresponding to points P_1 and P_2 are smaller than those of the original signals, which may present an additional problem for small signal-to-noise ratios. For this reason the estimation of the times of flight (ToF), in the current case, indicated as t_1 and t_2 in Fig. 12.17 based on which the location of the additional mass can be identified [1, 3], may be difficult and/or not precise due to the inherent dispersion of propagating wave signals. For this reason both ToFs are estimated assuming the signal threshold equal to 2% of its maximum value. In general, the poor sensitivity may be improved either by an increase in the carrier frequency f_c or alternatively by the use of more specialised damage indicators.

It can be checked that in the current case the distance l can be easily calculated from the following simple relationships:

$$\begin{cases} 2|P_1 P_2| = c_{g|f_2} t_1 \\ |P_1 P_3| = c_{g|f_2} t_2 \\ l = |P_1 P_2| - |P_1 P_3| \end{cases} \rightarrow l = c_{g|f_2} \left(t_2 - \frac{t_1}{2} \right) \quad (12.1)$$

which lead to the result of 182.3 mm, which is not too close to the assumed value of the distance l equal to 150 mm, giving the relative error of 21.5%.

⁵ A differential signal is understood here as a signal resulting from the difference between the signal obtained at a given point for the current but unknown state of a structure, and some reference signal obtained at the same point, but for a well-defined state of the structure.

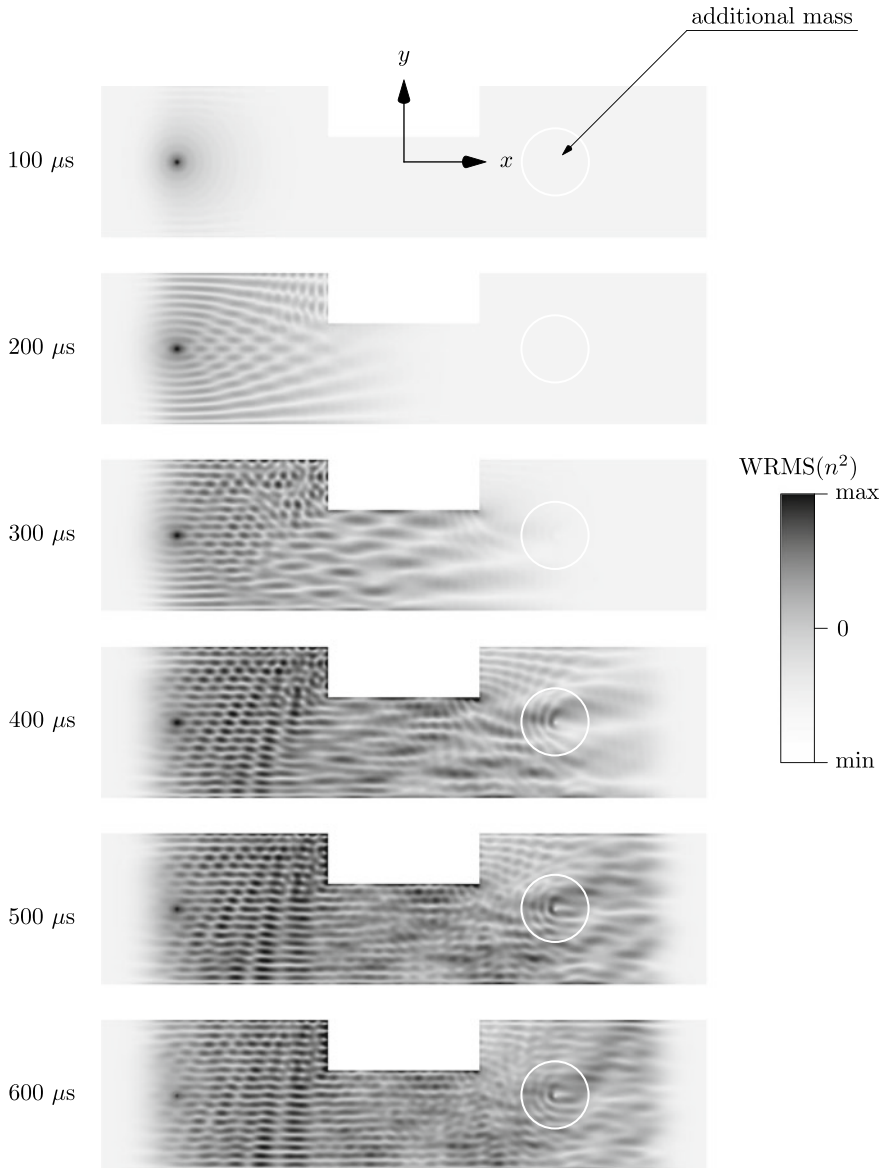


Fig. 12.18 $WRMS(n^2)$ patterns for the transverse acceleration component \ddot{u}_z according to the modified 3-mode 2-D theory of the antisymmetric behaviour of plates, obtained for a 10 mm thick infinite aluminium strip with a side cut-out. Results of numerical computations by TD-SFEM with NRBCs at infinity modelled by ALID

Of many damage indicators that can be possibly built and used, those which are based on the observation of the propagation of energy within a structure, rather than the observation of pure wave propagation patterns, seem particularly attractive. Typically a cumulative kinetic energy indicator or the root mean square (RMS) of measured time signals can be used for that purpose [1, 4]. It is noteworthy that damage indicators based on modified RMS, such as is a weighted root mean square (WRMS) for example, provide an increased sensitivity even in the case of damage of small magnitudes located at large distances from signal sources.⁶ The use of such an improved damage indicator in the form of $\text{WRMS}(n^2)$ is demonstrated in Fig. 12.18.

Thanks to this the location of the additional mass within the strip under consideration with a side cut-out becomes clearly visible as soon as the excited waves reach point P_2 , that is after initial 400 μs . In subsequent moments in time the obtained RMS patterns only become sharpened and amplified, which allows one to shorten the time of numerical analysis significantly. In the current case, according to results presented in Fig. 12.18, with no loss of accuracy the total calculation time T can be reduced by half from the initial 800 to 400 μs and from 6,400 equal time steps to 3,200.

It should be emphasised that for excitation signals broader in the frequency domain, which may lead to the propagation of other antisymmetric modes of SH-waves and Lamb waves than the fundamental A_0 mode of Lamb waves, other theories of antisymmetric behaviour of plates should be used, preferably multi-mode or higher-order multi-mode 3-D theories.

12.3 Wave Propagation in a Flanged Pipe with a Circumferential Crack

12.3.1 Problem Definition

The last numerical example concerns wave propagation in the most complex configuration, which is represented by an infinite flanged pipe section with a small circumferential crack.

As before, thanks to the application on NRBC only a finite section of the structure can be investigated. Its geometry is presented in Fig. 12.19. It is assumed that the flanged pipe section under consideration is made out of aluminium of the same material properties as before: Young's modulus E of 67.5 GPa, Poisson's ratio ν of 0.33 and material density of 2700 kg/m^3 , as summarised in Table 4.2 in Sect. 4.2.

⁶ For a discrete sequence u_1, u_2, \dots, u_n of n numbers a weighted RMS can be simply defined as $\text{WRMS}(w_n) = \sqrt{w_1 u_1^2 + w_2 u_2^2 + \dots + w_n u_n^2} / \sqrt{w_1 + w_2 + \dots + w_n}$, where w_n denote certain weights. In the case of $\text{WRMS}(1)$ the weights are assumed as $w_n = 1$ and $\text{WRMS}(1) \equiv \text{RMS}$, while in the case of $\text{WRMS}(n^2)$ the weights are assumed as $w_n = n^2$, thus $\text{WRMS}(n^2) = \sqrt{u_1^2 + 4u_2^2 + \dots + n^2 u_n^2} / \sqrt{1 + 4 + \dots + n^2}$.

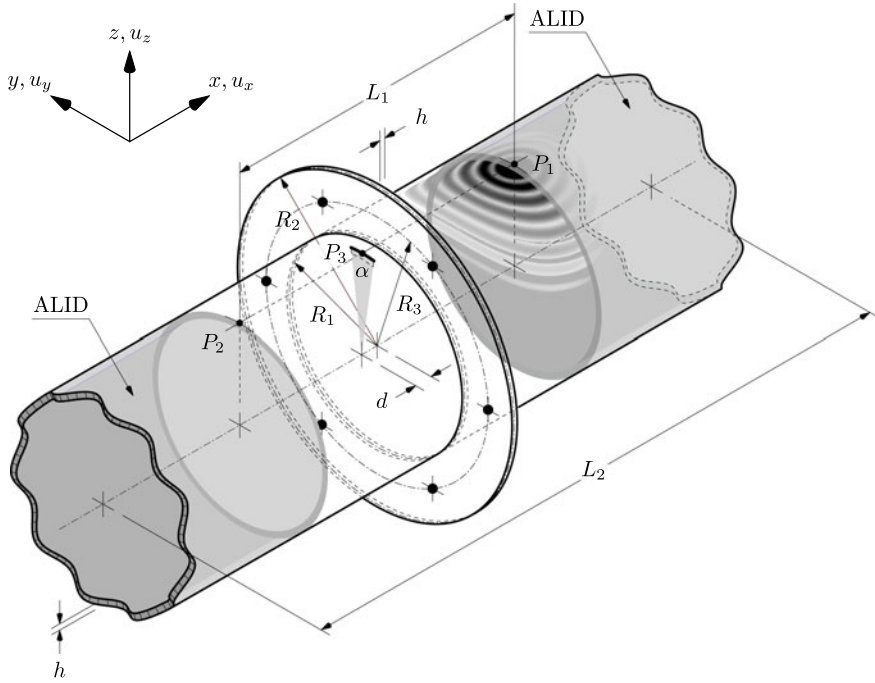


Fig. 12.19 Geometry of an aluminium flanged pipe section with a circumferential crack, with NRCBs at infinity modelled by ALID

The finite section of the pipe, having length L_1 of 500 mm, outer radius R_1 of 150 mm and thickness h of 10 mm, is of special interest. In the middle of this section a flange is located, having an outer radius R_2 of 250 mm and the same thickness h of 10 mm. On the flange face 6 evenly spaced M12 bolt sets are placed at a radius R_3 of 200 mm, represented by additional masses of 50 g each. Additionally, it is assumed that a small open circumferential crack, with its centre at point P_3 located at a distance d of 17 mm from the flange centre, is spanned over the angle α of 12° , which corresponds to its surface length of 31 mm. The crack is also assumed as open and a through-thickness crack.

The flanged pipe section of interest is indicated by points P_1 and P_2 , which are the points where dynamic responses are examined. The excitation signal is applied at point P_1 either as a transversely acting bending force leading to the generation of antisymmetric waves (antisymmetric excitation) or a transversely acting pair of tensile or compressive forces leading to the generation of symmetric waves (symmetric excitation), as discussed in [5]. It has the amplitude of 1 N and the form of 11 sine pulses of the carrier frequency f_c of 110 kHz, modulated by the Hann window, i.e. the frequency of modulation $f_m = f_c/m$ being equal to 10 kHz, where $m = 11$. As previously, the total calculation time T covers 800 μ s and is divided into 6400 equal time steps.

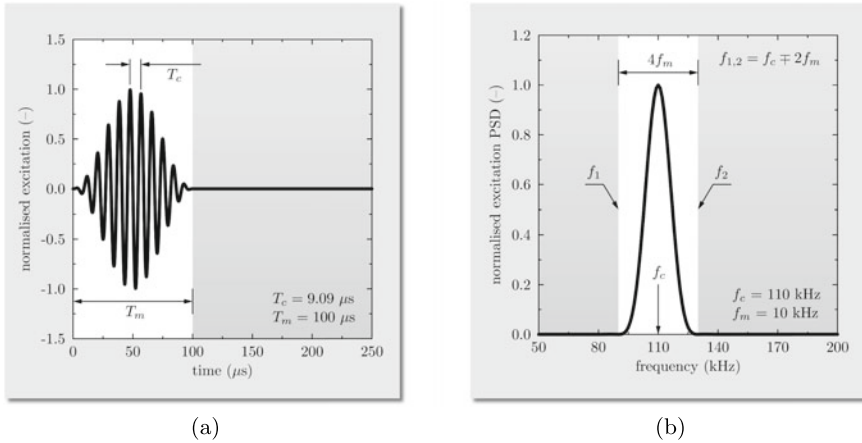


Fig. 12.20 Normalised excitation signal in: **a** the time domain, **b** the frequency domain

The excitation signal is presented in Fig. 12.20 in the time and frequency domains, for the initial 250 μs of its duration in the time domain and the frequency range from 50 kHz up to 200 kHz in the frequency domain.

12.3.2 Dispersion Curves and Theory Selection

In the current case, due to the geometry of the section under consideration as well as two excitation modes, the process of the theory selection must concern both symmetric and antisymmetric modes, which can propagate. As before the range of excited frequencies must be compared with the analytical dispersion curves already known from Sects. 5.1 and 5.2. This time, however, this process concerns the symmetric and antisymmetric modes of SH-waves and the Lamb waves, which can propagate within the structure, in order to select the most appropriate theories of symmetric and antisymmetric behaviour of plates/shells, which next can be employed for numerical computations.

From Figs. 12.20 and 12.21 it is evident that due to the assumed form of the excitation signal the excited waves within the section only concern three fundamental modes: the fundamental symmetric mode of Lamb waves S_0 , the fundamental antisymmetric mode of Lamb waves A_0 as well as the fundamental symmetric mode of SH-waves SH_0 , while the remaining symmetric and antisymmetric modes of SH-waves and Lamb waves are absent.

According to the analytical solutions presented in Sect. 5.2 the excited phase velocities for the fundamental symmetric mode of Lamb waves S_0 cover the range from 5.23 km/s at $f_1 = 90$ kHz down to 5.13 km/s at $f_2 = 130$ kHz, for the fundamental antisymmetric mode of Lamb waves A_0 from 2.23 km/s at $f_1 = 90$ kHz up to

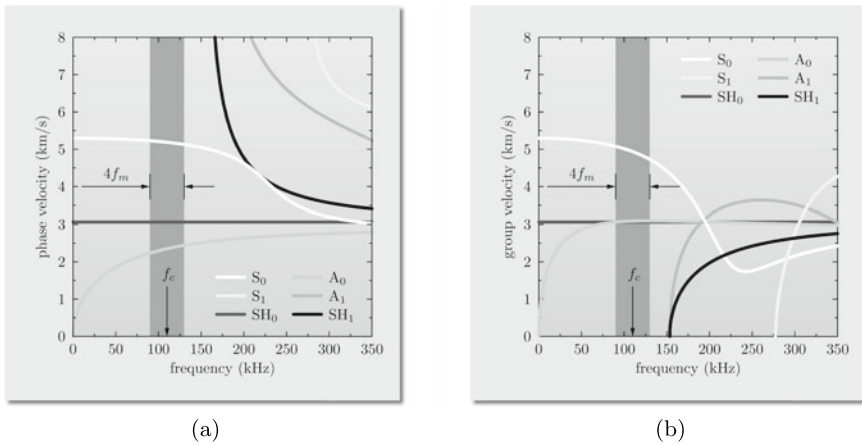


Fig. 12.21 Dispersion curves for: **a** the phase velocity, **b** the group velocity, for symmetric and antisymmetric modes of Lamb waves and SH-waves: S_0 , S_1 , A_0 , A_1 , SH_0 and SH_1 propagating in a 10mm thick aluminium flanged pipe section with a circumferential crack, according to the analytical solutions

2.44 km/s at $f_2 = 130$ kHz, while for the fundamental symmetric mode of SH-waves SH_0 , which is non-dispersive, it is constant and equal to 3.07 km/s for all frequencies. In the case of the group velocities the obtained values are different and for the fundamental symmetric mode of Lamb waves S_0 cover the range from 5.08 km/s at $f_1 = 90$ kHz down to 4.73 km/s at $f_2 = 130$ kHz, for the fundamental antisymmetric mode of Lamb waves A_0 from 3.07 km/s at $f_1 = 90$ kHz up to 3.10 km/s at $f_2 = 130$ kHz.

Based on Fig. 12.21 it can be concluded that the waves propagating as the fundamental modes in 2-D elastic space, which is the infinite flanged pipe section under investigation with a circumferential crack, are characterised by *moderate dispersion*, i.e. -1.9% of the relative change in the phase velocity and -6.9% in the group velocity in the case of the fundamental symmetric mode of Lamb waves S_0 and 9.4% of the relative change in the phase velocity and 1.0% in the group velocity in the case of the fundamental antisymmetric mode of Lamb waves A_0 . This is a direct consequence of the characteristic equations for the symmetric and antisymmetric modes of Lamb waves and SH-waves. This, together with the considerations from Sects. 8.1 and 8.2, as well as the results presented in Fig. 8.20, allows one to state that simple multi-mode theories of the symmetric and antisymmetric behaviour of plates appear sufficient for modelling purposes, as summarised in Tables 8.1 and 8.2.

In the same manner as before it can be noted that in the current case the upper frequency limit of the excitation signal is placed below the frequency corresponding to the first cut-off frequency for the first antisymmetric mode of SH-waves and Lamb waves, A_1 and SH_1 , $f_{A_1|SH_1}$ of 153.4 kHz. Based on the same reasoning as in the case of the previous numerical example, discussed in Sect. 12.2, it is decided to employ *the modified 6-mode 3-D theory of shells*. Of the simple theories discussed in Sects. 8.1

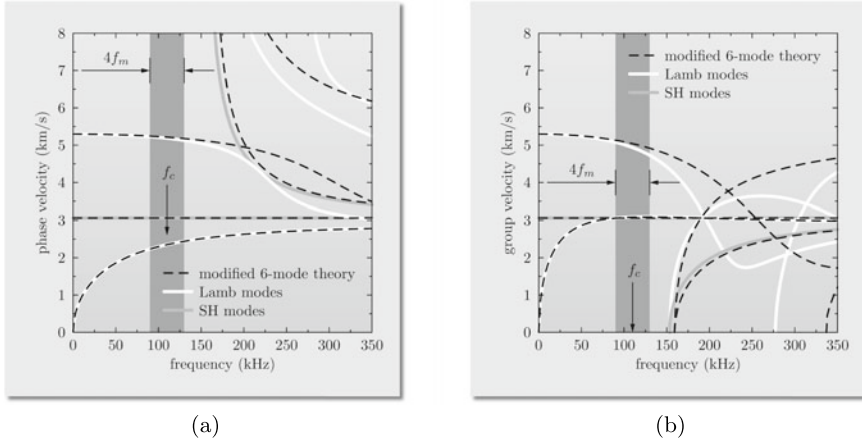


Fig. 12.22 Dispersion curves for: **a** the phase velocity, **b** the group velocity, for symmetric and antisymmetric modes of Lamb waves and SH-waves propagating in a 10 mm thick infinite aluminium flanged pipe section with a circumferential crack, according to the modified 6-mode 3-D theory of shells

and 8.2, the current theory, being a simple combination of the modified 3-mode theories of the symmetric and antisymmetric behaviour of plates, is characterised by a simple definition of its displacement field combined with a great accuracy in the frequency range of interest. As previously it should be emphasised that the values of the cut-off frequencies provided by analytical dispersion curves are always lower than the values obtained from simplified theories, thus providing a kind of safe margin in modelling.

The phase and group velocity dispersion curves obtained for the modified 6-mode theory of shells, for symmetric and antisymmetric modes of Lamb waves and SH-waves, are presented in Fig. 12.22. It can be clearly seen in Fig. 12.22 that within the range of excited frequencies the dispersion curves for the fundamental symmetric mode of Lamb waves S_0 , the fundamental antisymmetric mode of Lamb waves A_0 and the fundamental symmetric mode of SH-waves SH_0 , obtained for the selected modified 6-mode 3-D theory of shells, agree very well with the analytical dispersion curves obtained based on the corresponding characteristic equations.

It should be emphasised that based on the results presented in Fig. 12.22 the extreme values of the modelling errors can be easily assessed. In the case of the fundamental symmetric mode of Lamb waves S_0 the relative error associated with the phase velocity is very small with its value equal to 0.92% and its average value to 0.55%, while in the case of the fundamental antisymmetric mode of Lamb waves A_0 is negligible with its value equal to -0.06% and its average value equal to -0.04% . In the same manner the extreme values of the modelling errors associated with the group velocity are examined. As a result it can be stated that in the case of the fundamental symmetric mode of Lamb waves S_0 the relative error associated with the group velocity is small with its value equal to 3.92% and its average value equal to

2.21%, while in the case of the fundamental antisymmetric mode of Lamb waves A_0 is negligible with its value equal to -0.26% and its average value equal to -0.21% .

The modelling errors associated with the fundamental symmetric mode of SH-waves SH_0 is neglected in this analysis, since this wave mode is non-dispersive and as a consequence it fully conforms with the analytical dispersion curves obtained for the phase and group velocities.

12.3.3 ALID Parameters and Numerical Discretisation

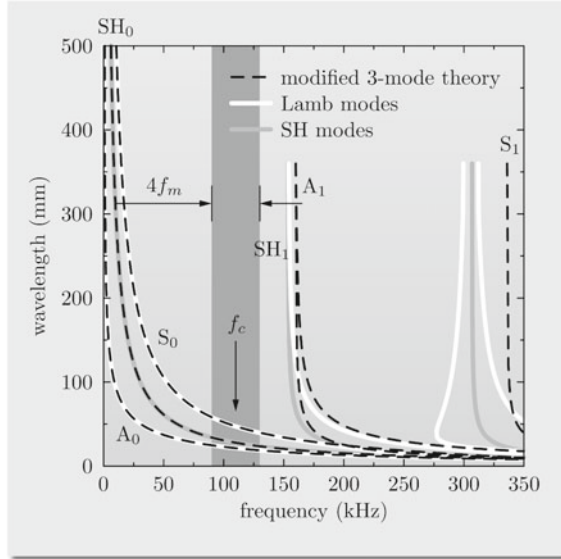
In order to model the infinite length of the flanged pipe section the same method is employed in the current case as in the case of the infinite aluminium strip, which is the technique of ALID, discussed in detail in Sect. 11.3. In the same manner as before it can be said that as a consequence of the use of ALID the numerical model of the pipe section must be extended accordingly to incorporate the presence of two damping layers, one at each end of the pipe section, as presented in Fig. 12.19. The depths of the layers must be defined as resulting not only from the frequency content of the excitation signal, but also as depending on the applied theory.

Once again, it can be stated that the knowledge of the range of the excited frequencies can be used not only to select the most appropriate theory of the shell behaviour or to establish the depth of ALID, but also to establish the requirements for the flanged pipe section discretisation conforming with the minimal number of nodal distances per wavelength. The dispersion curves for the wavelength for modes of Lamb waves and SH-waves, according to the modified 6-mode 3-D theory of shells, are presented in Fig. 12.23.

It can be clearly seen from Fig. 12.23 that the extreme wavelengths for the selected excitation signal and its frequency content must differ depending on the wave mode under consideration, since three fundamental modes of Lamb waves and SH-waves are present there. In the case of the fundamental symmetric mode of Lamb waves S_0 the corresponding values of the extreme wavelengths are the greatest and equal to $\lambda_{1|S_0} = 58.4$ mm at the frequency $f_1 = 90$ kHz and $\lambda_{2|S_0} = 39.8$ mm at the frequency $f_2 = 130$ kHz. In the case of the fundamental antisymmetric mode of Lamb waves A_0 the corresponding values of the extreme wavelengths are the smallest and equal to $\lambda_{1|A_0} = 24.8$ mm at the frequency $f_1 = 90$ kHz and $\lambda_{2|A_0} = 18.8$ mm at the frequency $f_2 = 130$ kHz. Consequently, in the case of the fundamental symmetric mode of SH-waves SH_0 the extreme wavelengths take intermediate values equal to $\lambda_{1|SH_0} = 34.1$ mm at the frequency $f_1 = 90$ kHz and $\lambda_{2|SH_0} = 23.6$ mm at the frequency $f_2 = 130$ kHz.

Since the depth of ALID must be defined using the knowledge about the longest wavelength in the frequency content of the excitation signal out of all modes available, it can be stated that in the current case this must be done based on the values related to the fundamental symmetric mode of Lamb waves S_0 . As before the depth of each damping layer is taken as a multiple of $\lambda_{1|S_0} = 58.3$ mm, so the assumed depth of ALID is $L = 4\lambda_1 \approx 234$ mm, with $p = 3$. For this reason the total length of

Fig. 12.23 Dispersion curves for the wavelength for modes of Lamb waves and SH-waves of a 10 mm thick infinite aluminium flanged pipe section with a circumferential crack, according to the modified 6-mode 3-D theory of shells



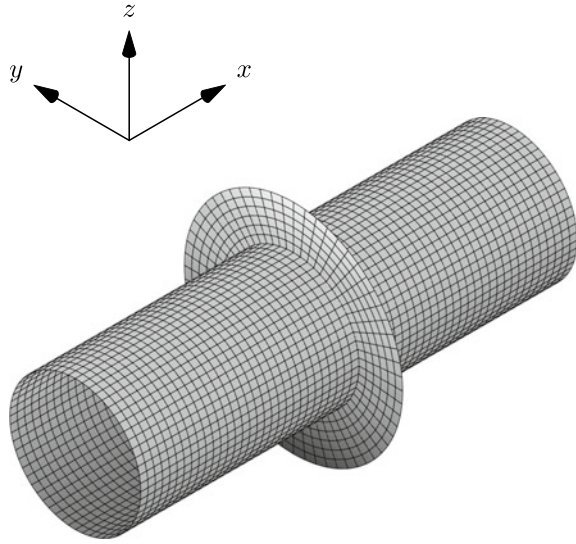
the flanged pipe section under consideration must be increased by at least $2L$ from $L_1 = 500$ mm to $L_2 = 968$ mm, which value is additionally increased to $L_2 = 1000$ mm in order to simplify the discretisation process.

It should be emphasised here that any changes in the excitation frequency f_c or the modulation frequency f_m must involve corresponding modifications to the depth of ALID in order to guarantee its optimal damping properties. Based on the established parameters of ALID and the requirements for shell discretisation a numerical model of the flanged pipe section under investigation with a circumferential crack can be finally built. For the purpose of the current analysis it is decided to use TD-SFEM and 36-node shell SFEs based on Lobatto nodes [1], as discussed in Sect. 8.3.

The knowledge of the corresponding shortest wavelengths obtained from Fig. 12.23 allows one to state, in a similar manner as in both previous numerical cases, that the requirement of 4 nodal distances per wavelength is satisfied only for the lengths of SFEs equal to, or shorter than, the wavelength $\lambda_{2|A_0} = 18.8$ mm.

Thus, it is decided to divide the strip into 3,960 shell SFEs, i.e. 60 SFEs along its length axis and 60 SFEs along its circumference, plus 360 SFEs used for modelling the flange, as presented in Fig. 12.24. As a result of the discretisation process the characteristic dimension of each SFE can be estimated as 16.6 mm, thus the number of nodal distances per wavelength secured by such a discretisation level can be estimated as approximately equal to 6 nodal distances per shortest wavelength. The resulting number of DOFs of the discrete numerical model is 595,854.

Fig. 12.24 The mesh of shell SFEs, according to the modified 6-mode 3-D theory of shells, used for numerical computations, consisting of 3,960 SFEs and 595,854 DOFs



12.3.4 Numerical Computations and Result Discussion

For numerical computations carried out the explicit method of central differences, as discussed in Sect. 10.7, is employed exactly in the same manner as in the case of the infinite aluminium strip with a side cut-off. The use of the explicit method of central differences enables one to take advantage of the diagonal form of the resulting global inertia matrix \mathbf{M} . However, it should be strongly emphasised here that in the case of the flanged pipe section under investigation the geometrical couplings resulting from non-flat geometry lead to certain off-diagonal elements in the global inertia matrix \mathbf{M} . Their magnitudes, being inversely proportional to the local radius of curvature, remain very small in comparison with the diagonal elements of this matrix and for this reason all off-diagonal elements in the global inertial matrix \mathbf{M} are neglected.

The spectrum of frequencies of free vibrations of the flanged pipe section is also not examined due to the 3-D nature of the section and resulting couplings of normal modes, which significantly complicate, or simply prevent, such an analysis in comparison with 1-D cases. For the very same reason also the performance of ALID is not tested. However, this performance can be estimated based on the methodology presented before and concerning the results obtained in the case of the 1-D infinite stepped aluminium bar.

The knowledge of the established parameters of the discrete numerical model of the flanged pipe section under consideration allows one to compute its dynamic responses. They are presented in Figs. 12.25 and 12.26 as wave propagation patterns at selected moments in time for the amplitudes of the resulting acceleration components $AMP^2 = \ddot{u}_x^2 + \ddot{u}_y^2 + \ddot{u}_z^2$, for both types of excitation. It can be expected that the interaction of propagating waves with structural discontinuities in the form of

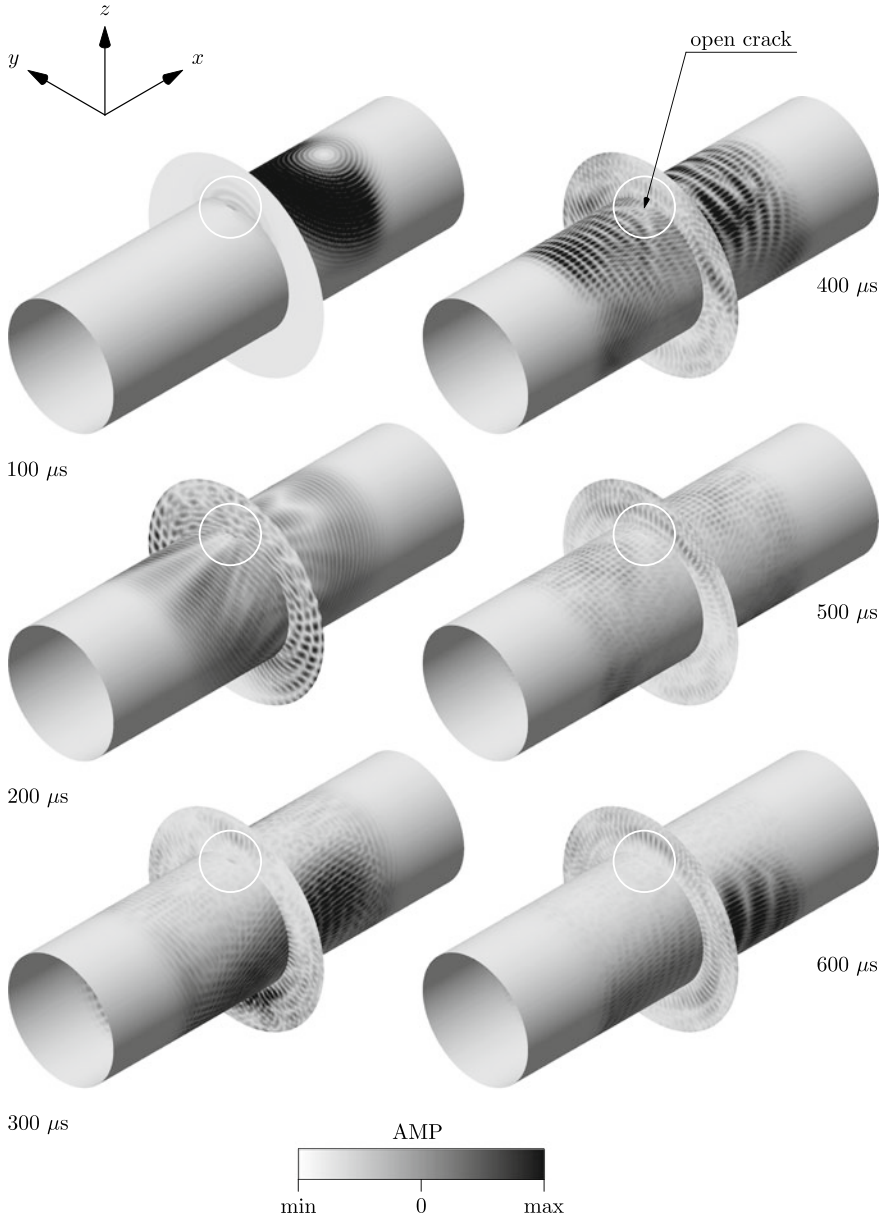


Fig. 12.25 Wave propagation patterns for the amplitude of the resulting acceleration component AMP according to the modified 6-mode 3-D theory of shells, obtained for an aluminium flanged pipe section with a circumferential crack in the case of antisymmetric excitation. Results of numerical computations by TD-SFEM with NRBCs at infinity modelled by ALID

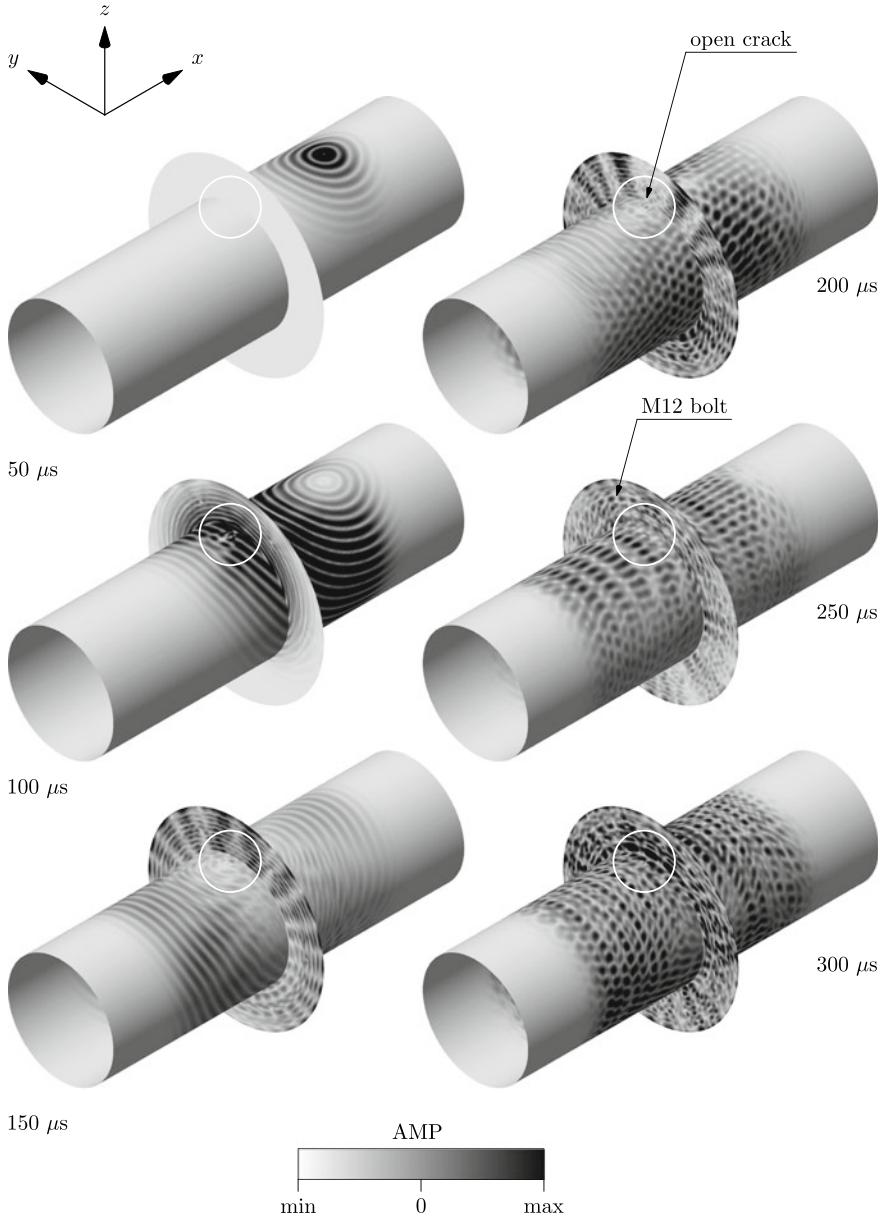


Fig. 12.26 Wave propagation patterns for the amplitude of the resulting acceleration component AMP according to the modified 6-mode 3-D theory of shells, obtained for an aluminium flanged pipe section with a circumferential crack in the case of the symmetric excitation. Results of numerical computations by TD-SFEM with NRBCs at infinity modelled by ALID

the crack and bolts should influence the observed patterns in such a way that their locations are revealed. However, from the results presented in Figs. 12.25 and 12.26 this is not evident.

The reason for such behaviour may seem to lie in too small sensitivity of the propagating waves to structural damage/discontinuity. This sensitivity may be estimated as proportional to the shortest wavelength out of all wavelengths constituent in the propagating waves and resulting from the assumed form of the excitation signal, but it also depends on the type of excitation [1, 6, 7]. In the case of antisymmetric excitation the shortest wavelengths is $\lambda_{2|A_0} = 18.8$ mm, while in the case of symmetric excitation it is $\lambda_{2|S_0} = 39.8$ mm. Despite the fact of mode conversion between symmetric and antisymmetric modes at the flange position the response of the pipe section is dominated by the type of excitation. For this reason, at least in the case of the antisymmetric excitation, since the crack length of 31 mm is grater than the shortest wavelength, the location of the crack should be clearly revealed. However, this is not visible in either case of excitation except the early stage of development of wave propagation patterns, as seen in Fig. 12.25 at 200 μs and Fig. 12.26 at 100 μs . Alternatively, the problem may also be related to too complicated wave propagation patterns, which are very difficult to interpret due to multiple reflections and/or possible mode conversion. This problem is very well illustrated by Figs. 12.27 and 12.28, for both types of excitation, where the obtained dynamic responses are compared at points P_1 and P_2 . As previously it should be pointed out that the dynamic responses obtained at point P_1 are initially dominated by the excitation. For this reason it is decided to exclude the time window corresponding to the time of excitation, which is equal to the modulation time T_m of 100 μs .

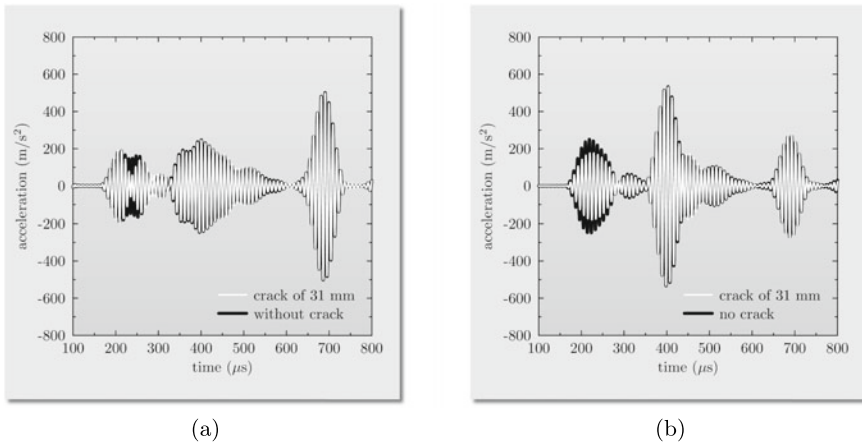


Fig. 12.27 Dynamic responses for the transverse acceleration component \ddot{u}_x taken at: **a** point P_1 , **b** point P_2 , of an aluminium flanged pipe section with a circumferential crack in the case of the antisymmetric excitation, according to the modified 6-mode 3-D theory of shells. Results of numerical computations by TD-SFEM with NRBCs at infinity modelled by ALID

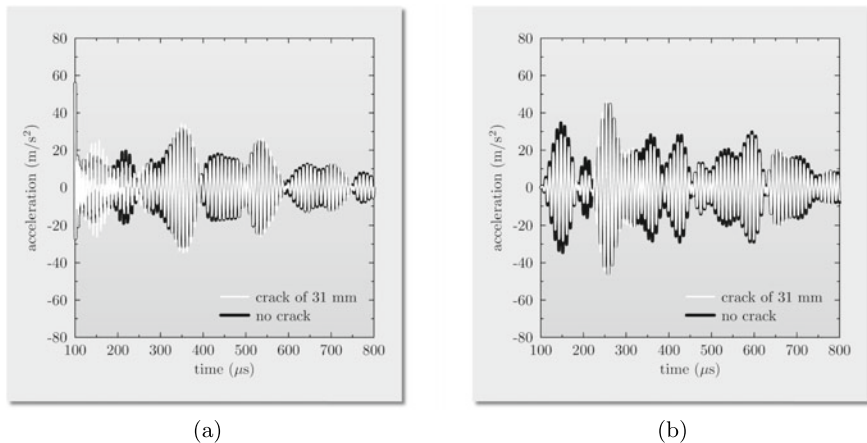


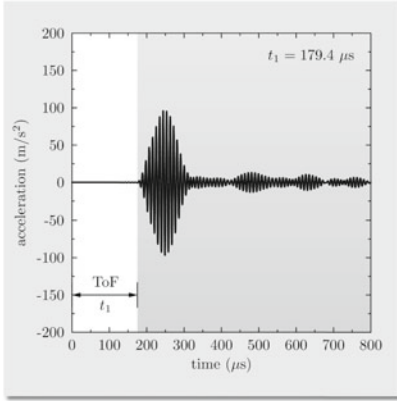
Fig. 12.28 Dynamic responses for the transverse acceleration component \ddot{u}_x taken at: **a** point P_1 , **b** point P_2 , of an aluminium flanged pipe section with a circumferential crack in the case of the symmetric excitation, according to the modified 6-mode 3-D theory of shells. Results of numerical computations by TD-SFEM with NRBCs at infinity modelled by ALID

It can be seen from Figs. 12.27 and 12.28 that within the time signals corresponding to points P_1 and P_2 there is no clear evidence of any reflections resulting from the presence of the crack, which on the other hand is the effect of signal reflections/conversion at the flange position. Despite the fact that the signals obtained for the cases when the crack is present or not must be different, it is impossible to directly extract from them any useful information about the location of the crack.

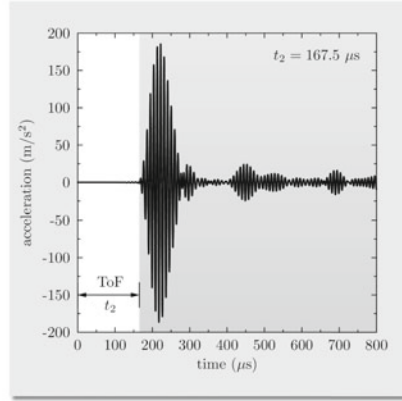
This adverse situation is not significantly improved when differential signals are examined, as shown in Figs. 12.29 and 12.30, for the same two types of excitation. It is clear that the amplitudes of the differential signals corresponding to points P_1 and P_2 are smaller than those of the original signals, which may present a problem for small signal-to-noise ratios. For this reason the estimation of the times of flight (ToF), in the current case indicated as t_1 and t_2 in Figs. 12.29 and 12.30, based on which the location of the additional mass can be evaluated [1, 3], is difficult and/or not precise due to the inherent dispersion of propagating wave signals. Both ToFs are estimated assuming the same signal threshold equal to 2% of its maximum value. In the same manner as before the poor sensitivity may be improved either by an increase in the carrier frequency f_c or alternatively by the use of more specialised damage indicators.

It can be checked that in the current case the distance d can be easily calculated from the following simple relationships:

$$\begin{cases} 2|P_1 P_3| = c_{g|f_2} t_1 \\ |P_1 P_2| = c_{g|f_2} t_2 \\ 2d = 2|P_1 P_3| - |P_1 P_2| \end{cases} \rightarrow d = c_{g|f_2} \left(\frac{t_1 - t_2}{2} \right) \quad (12.2)$$

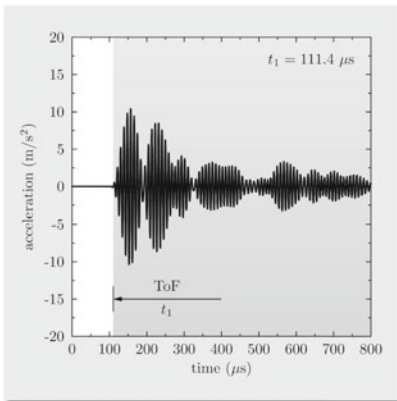


(a)

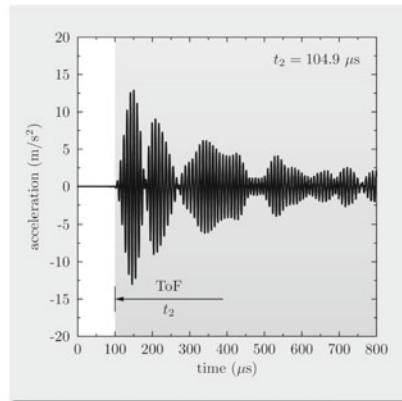


(b)

Fig. 12.29 Differential signals for the transverse acceleration component \ddot{u}_x taken at: **a** point P_1 , **b** point P_2 , of an aluminium flanged pipe section with a circumferential crack in the case of the antisymmetric excitation, according to the modified 6-mode 3-D theory of shells. Results of numerical computations by TD-SFEM with NRBCs at infinity modelled by ALID



(a)



(b)

Fig. 12.30 Differential signals for the transverse acceleration component \ddot{u}_x taken at: **a** point P_1 , **b** point P_2 , of an aluminium flanged pipe section with a circumferential crack in the case of the symmetric excitation, according to the modified 6-mode 3-D theory of shells. Results of numerical computations by TD-SFEM with NRBCs at infinity modelled by ALID

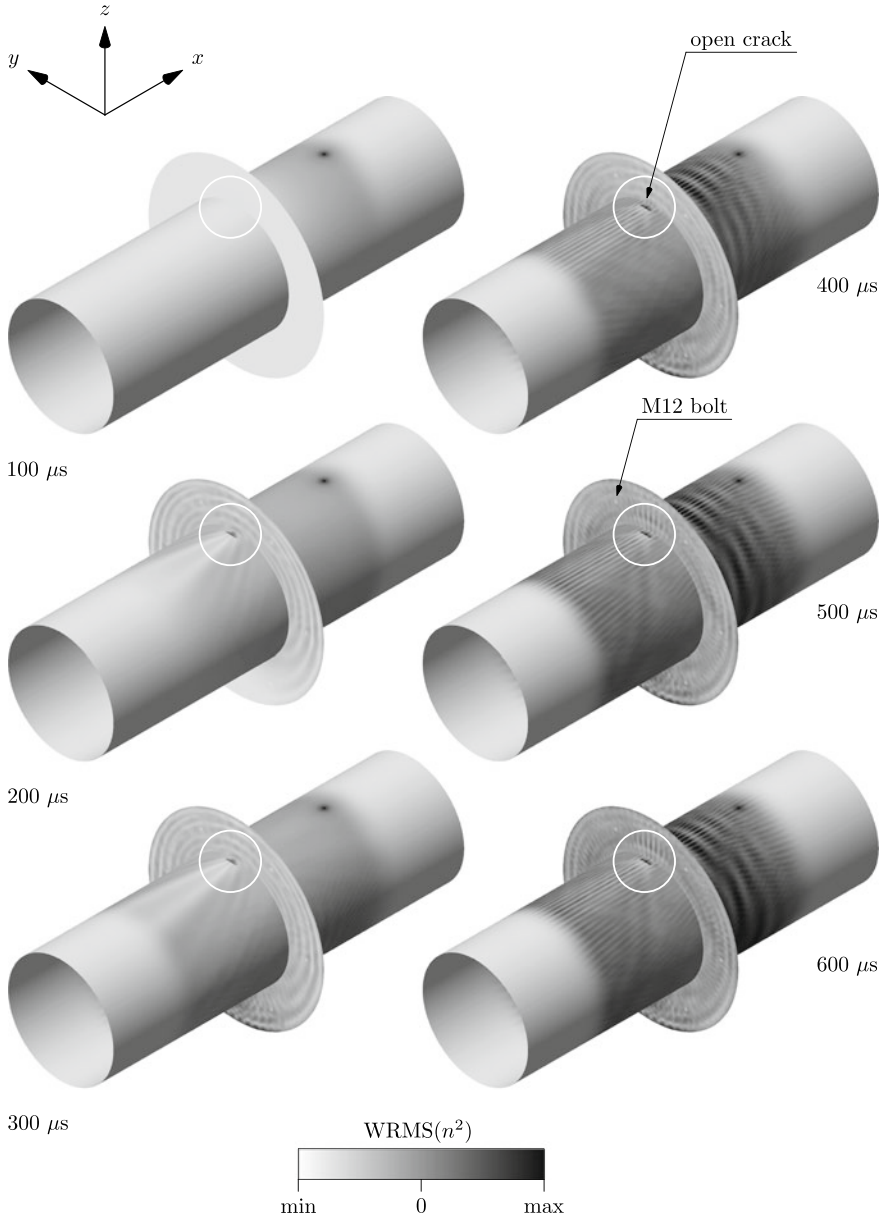


Fig. 12.31 $\text{WRMS}(n^2)$ patterns for the amplitude of the resulting acceleration component AMP according to the modified 6-mode 3-D theory of shells, obtained for an aluminium flanged pipe section with a circumferential crack in the case of the antisymmetric excitation. Results of numerical computations by TD-SFEM with NRBCs at infinity modelled by ALID

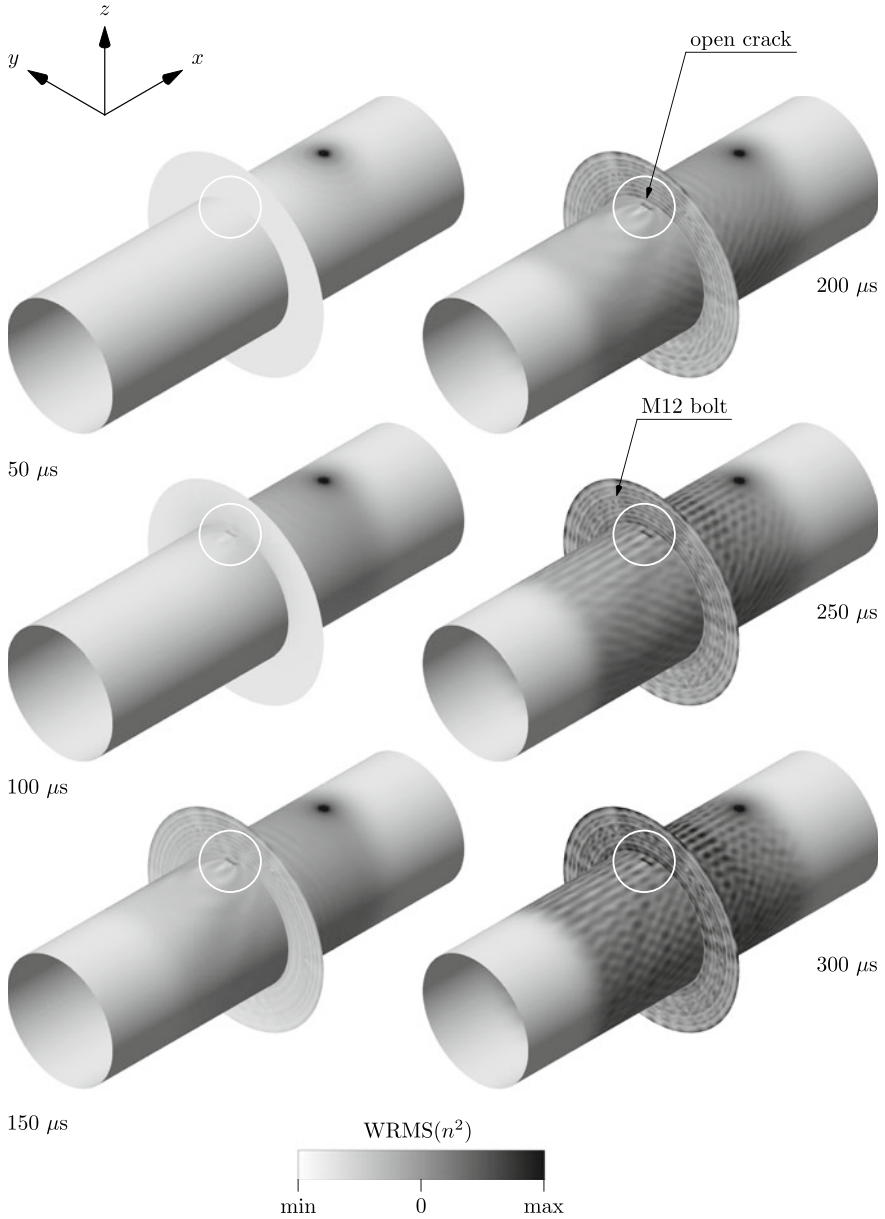


Fig. 12.32 WRMS (n^2) patterns for the amplitude of the resulting acceleration component AMP according to the modified 6-mode 3-D theory of shells, obtained for an aluminium flanged pipe section with a circumferential crack in the case of the symmetric excitation. Results of numerical computations by TD-SFEM with NRBCs at infinity modelled by ALID

which lead to the result of 18.5 mm in the case of antisymmetric excitation and of 16.0 mm in the case of symmetric excitation. The obtained results stay close to the assumed value of the distance d equal to 17 mm with the relative error of 8.5% and -5.5% , respectively.

In the very same manner as before, in order to precisely pinpoint the location of the crack, the damage indicator in the form of $WRMS(n^2)$ is employed as presented in Figs. 12.31 and 12.32. Thanks to this the location of the crack within the flanged pipe section under consideration with a circumferential crack becomes easily visible as soon as the excited waves reach point P_2 , that is well before the initial 400 μs . At the same time the locations of the bolts are also revealed.

It can be also noted that the interaction of propagating waves with the crack leads to more prominent patterns revealing the crack location in the case of the antisymmetric excitation than in the case of the symmetric excitation. The behaviour observed is explained based on the same analysis of the characteristic wavelengths associated with both types of excitations already given. Consequently, in the case of the symmetric excitation these wavelengths are much greater due to the greater values of the phase and group velocities associated with the fundamental symmetric mode of Lamb waves S_0 , as clearly seen from Fig. 12.23. Thus, the resulting sensitivity to damage is smaller than in the case of the antisymmetric excitation.

As before, it can be observed that in consecutive moments in time the obtained RMS patterns only become sharpened and amplified, which allows one to shorten the time of numerical analysis significantly. In the current case, according to results presented in Figs. 12.31 and 12.32, with no loss of accuracy the total calculation time T can be reduced by half from the initial 800 to 400 μs and from 6,400 equal time steps to 3,200.

It should be emphasised that for excitation signals broader in the frequency domain, which may lead to the propagation of other symmetric or antisymmetric modes of Lamb waves and SH-waves than the fundamental modes S_0 , A_0 and SH_0 mode other theories of shell behaviour should be used, preferably multi-mode or higher-order multi-mode 3-D theories.

References

1. W. Ostachowicz, P. Kudela, M. Krawczuk, and A. Żak. *Guided waves in structures for SHM. The time-domain spectral element method*. John Wiley & Sons Ltd., Singapore, 2012.
2. A. Żak, M. Krawczuk, Ł. Skarbek, and M. Palacz. Numerical analysis of elastic wave propagation in unbounded structures. *Finite Elements in Analysis and Design*, 90:1–10, 2014.
3. W. Ostachowicz, M. Krawczuk, A. Żak, and P. Kudela. Damage detection strategies in elements of structures by the elastic wave propagation method. *Computer Assisted Mechanics and Engineering Sciences*, 13:109–204, 2006.
4. A. Żak, M. Radziński, M. Krawczuk, and W. Ostachowicz. Damage detection strategies based on propagation of guided elastic waves. *Smart Materials and Structures*, 21:1–18, 2012.
5. A. Żak. A novel formulation of a spectral plate element for wave propagation in isotropic structures. *Finite Element in Analysis and Design*, 45:650–658, 2009.

6. V. Giurgiutiu. *Structural health monitoring of aerospace composites*. Academic Press, Oxford, 2016.
7. J. L. Rose. *Ultrasonic waves in solid media*. Cambridge University Press, Cambridge, 1999.